UCRL-16918

University of California

Ernest O. Lawrence Radiation Laboratory

HIGH-ENERGY NUCLEON-NUCLEON SCATTERING FROM REGGE POLES

Berkeley, California

DISCLAIMER

Submitted to Physical Review for publication

UCRL-16918
Preprint

UNIVERSITY OF CALIFORNIA
Lawrence Radiation Laboratory
Berkeley, California

AEC Contract No. W-7405-eng-48

HIGH-ENERGY NUCLEON-NUCLEON SCATTERING FROM REGGE POLES

Victor Flores-Maldonado

June 8, 1966

TECHNICAL INFORMATION DIVISION

Lawrence Radiation Laboratory

Berkeley

Assigned to INFORMATION DIVISION

Route to	Noted
O. N. Larsen	AUG 18 1966
V. Franco	SEP 11 1967

Please return this document to the Information Division. Do not send it to the next person on the list.

Please do not remove this page.

RL-254-1

HIGH-ENERGY NUCLEON-NUCLEON SCATTERING FROM REGGE POLES.*

Victor Flores-Maldonado†

Department of Physics and Lawrence Radiation Laboratory
University of California
Berkeley, California

June 8, 1966

ABSTRACT

A phenomenological study of N-N scattering is made according to the Regge pole theory. The p-p , $\bar{p}$-p , p-n , and $\bar{p}$-n elastic processes and p-n , and $\bar{p}$-n charge-exchange scattering are considered. The purpose of this work is twofold. First, to see if there is agreement between a simple Regge pole model and the existing experimental data, such as measurements of σ_t, $d\sigma/dt$, polarizations, ratio of the real to the imaginary parts of the amplitude, and other inferences from π-N scattering. Second, if agreement is found, to investigate the behavior of the trajectories and residue functions. It is found that a Regge pole model which includes the contributions of the trajectories P , P' , ω , ρ , and R can account for the data. The agreement is better above 15 $(\text{GeV})^2$. Below this energy, discrepancies between this model and experimental data begin to be noticed. This happens, in particular, in processes in which ρ and R are the principal contributors. We find that the zero-momentum-transfer data are in good agreement with an ω intercept of 0.5 , with P , P' , and ω residues almost equal in value, and with comparatively small ρ and R residues. The study of the

data at invariant moment transfers less than zero indicates that the trajectories are straight lines or have a small curvature. They seem to follow the trend of the Chew-Frautschi diagram. Poor agreement is obtained with trajectories that tend asymptotically to the axis, $\alpha = 0$. The residues of the trajectories of even signature, P, P', and R, behave similarly. They remain greater than or equal to zero, this latter value at the point at which the corresponding trajectory crosses the axis $\alpha = 0$. In contrast, the residues of the trajectories of odd signature, ω and ρ, pass to the negative side of the plane at momentum transfers of about $-0.1\ (\mathrm{GeV})^2$. They remain less than or equal to zero, this latter value at the point at which the corresponding trajectory crosses the axis $\alpha = -1$. The physical constraints of unitarity, spin structure, factorization, and assumption of real analyticity of the residues are imposed.

I. INTRODUCTION

A two-particle interaction is conveniently described by transition amplitudes between initial and final states of definite momenta and spin.[1] The concept of analyticity allows the connection of the amplitudes of one channel in terms of the amplitudes of another channel, simply by analytic continuation. This idea is useful for constructing invariant amplitudes at relativistic energies, where the potential approximation cannot be used. The amplitudes may be written in terms of the square of the center-of-mass (c.m.) energy of connected channels.

For the direct (s) channel in $N\text{-}N \to N\text{-}N$ scattering, the amplitude may be expressed in terms of the energy invariant, $s = 4(p_s^2 + m^2)$, and the momentum-transfer invariant, $t = -2p_s^2(1 - z_s)$, where p_s is the c.m. momentum of one of the nucleons, m is the nucleon mass, and z_s is the cosine of the c.m. scattering angle. The other energy invariant, $u = -2p_s^2(1 + z_s)$, can be written in terms of s and t by use of the relation $s + t + u = 4m^2$. For the crossed (t) channel one has $N\text{-}\bar{N} \to N\text{-}\bar{N}$ scattering and the similar expressions, $t = 4(p_t^2 + m^2)$, $u = -2p_t^2(1 - z_t)$, and $s = -2p_t^2(1 + z_t)$, with similar definition of p_t and z_t.

The scattering in the direct channel may be obtained from properties of the crossed annihilation channel. To this end the amplitudes are written also as a function of complex angular momentum.[2] The domain of interest is that of high energies (s) and small momentum transfer (t), where the Regge pole approximation is

applicable.[3] In this model the scattering is controlled by the exchange of total angular momentum trajectories of well-defined quantum numbers (in this case those of the $N\text{-}\bar{N}$ crossed channel) and J parity, since the angular momentum is interpolated.

The Regge pole theory has successfully correlated numerous experimental results. This success provides encouragement to study phenomenologically the $N\text{-}N$ experiments from this point of view. The data available consist mainly of total cross sections, differential cross sections, and polarizations. There are also some measurements of the ratio of the real to the imaginary parts of the amplitude in the forward direction.

In Section II, we compile the formulas to treat the four cases of elastic scattering, and $p\text{-}n$ and $\bar{p}\text{-}n$ charge exchange. The complete spin structure is considered, e.g., for each isotopic spin value, the five amplitudes are calculated exactly. In this form we avoid the uncertainties of simplified formulations based on only two independent amplitudes. We fit the data to investigate the unknown quantities of the theory, e.g., the trajectories and the residue functions.

In Section III, we consider the forward direction, where there is more theoretical and experimental information. After fitting the data we deal with the s region of applicability of the model and about the relevance of considering several trajectory contributions. This is of special interest, since the one-pole approximation is often used.

We treat in Section IV the region of momentum transfers different from zero. Here trajectories and residue functions are specified in accordance with experiment and with physical constraints, such as factorization and real analyticity of the residues.

The p-n and $\bar{p}$-n charge exchange are considered in Section V. The parameters relevant to these processes are determined. Their role in connection with elastic N-N scattering is discussed.

II. FORMULATION

A. Elastic Scattering

We are interested in the theoretical interpretation of the total cross section, σ_t, the differential cross section, $d\sigma/dt$, and the polarization, P. These quantities are functions of the variables s and t, the four-vector invariants in the direct and crossed channels respectively. With respect to elastic scattering, the four N-N cases in which we are interested will be specified by two indices, the isotopic spin, I, and the baryon number of the system, A. In this notation we have, for example,

$$\sigma_t(pp) \equiv \sigma_t(1,2)$$

$$\sigma_t(p,n) \equiv \sigma_t(0,2)$$

$$\sigma_t(\bar{p}p) \equiv \sigma_t(1,0)$$

$$\sigma_t(\bar{p}n) \equiv \sigma_t(p\bar{n}) \equiv \sigma_t(0,0) \quad .$$

The expressions that give the functions mentioned above take a simple form when they are expressed in terms of the helicity amplitudes, Φ_i, of which there are five due to the spin 1/2 of the nucleons. In this form, one may write[4,5]

$$\sigma_t(I,A) = 4\pi(s - 4m^2)^{-1/2} Im[\Phi_1(t = 0) + \Phi_3(t = 0] \quad , \quad (1)$$

$$\frac{d\sigma}{dt}(I,A) = \frac{2\pi}{s - 4m^2}(|\phi_1|^2 + |\phi_2|^2 + |\phi_3|^2 + |\phi_4|^2 + 4|\phi_5|^2) , \quad (2)$$

$$P(I,A)\frac{d\sigma}{dt}(I,A) = \frac{4}{s - 4m^2} \mathrm{Im}[(\phi_1 + \phi_2 + \phi_3 - \phi_4)\phi_5^*] , \quad (3)$$

where m is the nucleon mass. We use units $\hbar = c = 1$.

The amplitudes can, in turn, be expressed in terms of the individual trajectory contributions in the form

$$\phi_i(I,A) = \sum_{L=1}^{N} (2\alpha_L + 1)\zeta_L \phi_{iL}(I,A) . \quad (4)$$

In this equation, L designates the particle pole, N represents the number of trajectory contributions, $\phi_{iL}(I,A)$ is a function which takes into account the spin and isospin factors, α_L is a function of t that stands for the L pole trajectory, and ζ_L is the signature factor given by

$$\zeta_L = \frac{1 + \tau \exp(-i\pi\alpha_L)}{2 \sin \pi\alpha_L} , \quad (5)$$

where τ is the P parity or signature defined by $\tau = (-1)^J$, and J is the total angular momentum. Therefore, τ may have the values ± 1. When τ is $+1$, one has the case of an even-signature trajectory, whose particle pole becomes an actual particle when J is even, and when τ is -1, one has an odd-signature trajectory which is associated with particles of odd angular momentum.

The functions $\phi_{iL}(s,t)$ that are defined in Eq. (4) can now be expressed as a function of the amplitudes, $f_{jL}(s,t)$, of the crossed channel, that is, of the channel in which the invariant moment t becomes the square of the c.m. energy. They are so expressed because the f_{jL} amplitudes are related in a simple way to the pole trajectories that dominate the scattering process. In this form the individual trajectory contributions can be more readily identified. The connection between a state $\bar{N}$-$N(I',0)$ of the crossed channel and a state N-$N(I,2)$ of the direct channel can be written in terms of $\phi_{iL}(s,t)$ and $f_{jL}(s,t)$ in the form

$$\phi_{iL}(I,2) = \frac{(-1)^{I} B_{II'} s^{-1/2}}{(4m^2 - s)(4m^2 - t)} \sum_{j}^{5} K_{ij} f_{jL}(I',0) \quad , \tag{6}$$

where K_{ij} is the spin-space element of the transformation, and $B_{II'}$, the isotopic spin space factor. The $\bar{N}$-$N(I,0)$ to N-$N(I,2)$ crossing matrices are[6]

$$K = \begin{vmatrix} 0 & 4m^2u & 4m^2u-2s(t+u) & -\frac{4m^2u(s+u)+2s^2t}{s+u} & \frac{4stu}{s+u} \\ (s+u)(t+u) & -st & 4m^2u & \frac{4m^2u(s-u)}{s+u} & \frac{4stu}{s+u} \\ 0 & 4m^2u & u(s-t-u) & \frac{u[4m^2(s+u)+2st]}{s+u} & \frac{4stu}{s+u} \\ (s+u)(t+u) & st & -4m^2u & \frac{4m^2u(u-s)}{s+u} & -\frac{4stu}{s+u} \\ 0 & -2m(stu)^{\frac{1}{2}} & -2m(stu)^{\frac{1}{2}} & \frac{2m(stu)^{\frac{1}{2}}(u-s)}{s+u} & \frac{(stu)^{\frac{1}{2}}(4m^2u-st)}{m(s+u)} \end{vmatrix} \tag{7}$$

and

$$B = \begin{array}{c} \begin{array}{cc} I'=0 & I'=1 \end{array} \\ \left| \begin{array}{cc} -1/2 & 3/2 \\ 1/2 & 1/2 \end{array} \right| \begin{array}{c} I=0 \\ I=1 \end{array} \end{array} \tag{8}$$

where u, the four-vector invariant of the u channel, can be written as a function of s and t, with the use of the energy equation, $4m^2 = s + t + u$.

The prescription for obtaining $\phi_{iL}(I,0)$ must now be given to cover the remaining cases; beforehand, however, we digress briefly to see which trajectory contributions should be considered. First, they have to be able to communicate with the crossed channel; therefore, they must have quantum numbers equal to those of the $\bar{N}$-N annihilation channel. Second, they must be high-lying trajectories, since the scattering process at high energy is dominated by them. Some of the trajectories associated with the nonets $J^P = 2^+$ and $J^P = 1^-$ fulfill these requirements. They are listed in Table I. For these particular groups of trajectories the ordinary parity, P, and the J parity are equal,[6] and we will simply denote a trajectory of this type by the indices (L, τ, I'). It is not known at present whether the trajectory of maximal strength required to explain the total cross sections at the asymptotic high-energy limit is, or is not, the singlet member of the 2^+ nonet. If it is not, in addition to the Pomeranchuk trajectory of Table I, one should include a trajectory associated with f'(1525).

The π , ϕ , η , and A_1 trajectories also communicate with the $\bar{N}$-N channel. Nevertheless, they lie lower than those listed in Table I, and for this reason their contributions are less important at high energies. This statement will become more apparent in the following sections, where the possible relevance of some of them will be considered.

Finally we return to write the expression that gives $\phi_{iL}(I,0)$ for the trajectories P , P' , ω , ρ and R of Table I. In terms of $\phi_{iL}(I,2)$, we can write simply

$$\phi_{iL}(I,0) = \tau\phi_{iL}(I,2) \quad . \tag{9}$$

This expression is not general; it is meant for the trajectories of Table I only. For the arguments necessary to go from a state (I,2) to a state (I,0) see, for example, Ref. 8.

The functions $f_{iL}(t)$ that appear in Eq. (6) are partial waves of definite total angular momentum, total spin, S , and parity. One may therefore associate them with definite pole trajectories. They are obtained in the following manner. First, the amplitudes of the crossed channel, $f_i(t)$, are expanded in partial waves in the form[7,8]

$$f_1 = \frac{E_t}{P_t} \sum_J (2J+1) f^J_{00}(t) P_J(Z) \quad ,$$

$$f_2 = \frac{E_t}{P_t} \sum_J (2J+1) f^J_{11}(t) P_J(Z) \quad ,$$

$$f_3 = \frac{E_t}{P_t} \sum_J \frac{2J+1}{J(J+1)} \left\{ f_{33}^J(t) \left[P_J'(Z) + ZP_J''(Z) \right] - f_{22}^J(t) P_J''(Z) \right\} ,$$

$$f_4 = \frac{E_t}{P_t} \sum_J \frac{2J+1}{J(J+1)} \left\{ f_{22}^J(t) \left[P_J'(Z) + ZP_J''(Z) \right] - f_{33}^J(t) P_J''(Z) \right\} , \qquad (10)$$

$$f_5 = -\frac{m}{P_t} \sum_J (2J+1) \left[J(J+1) \right]^{-1/2} f_{12}^J(t) P_J'(Z) ,$$

where E_t and P_t are the c.m. energy and momentum respectively, and Z is the cosine of the c.m. scattering angle in the t channel. They may be expressed in the form, $P_t = 1/4(t - 4m^2)$, $E_t^2 = t/4$, and $Z = (2s/4m^2 - t) - 1$. The transition amplitudes between the possible $\bar{N}$-N states of the crossed channel are represented by $f_{00}^J(t)$, $f_{11}^J(t)$, $f_{22}^J(t)$, $f_{12}^J(t)$, and $f_{33}^J(t)$. The indices indicate the states between which the transitions take place. This is shown in more detail in Table II.[4,7,9]

The states $|0>$ and $|3>$ are conserved; $|0>$ is a singlet state and does not communicate with the triplet states and $|3>$ does not communicate with $|1>$ and $|2>$ because of P conservation. On the other hand, there is communication between the states $|1>$ and $|2>$. This has the following implication: in the Regge pole model it is assumed that the scattering is governed by simple poles, and if this is the case, it can be shown that because of unitarity the relation

$$f_{11}^J(t) f_{22}^J(t) \approx f_{12}^J(t)^2 \qquad (11)$$

should be valid.[10] Therefore, the transition probability between the states $|1>$ and $|2>$ is determined by this equation.

The quantum numbers of trajectories relevant to N-N scattering are given in Table III. The comparison of Tables II and III shows that trajectories of the type $P\tau = +1$, $s = 1$ -- e.g., P, P', ω, Φ, ρ, and R -- are associated with the transition amplitudes f_{11}, f_{22}, and f_{12}; trajectories of the type $P\tau = -1$, $s = 0$ -- e.g., π, η, and X^o -- are associated only with f_{00}, and trajectories of the type $P\tau = -1$, $s = 1$ -- e.g., A_1 -- are associated only with f_{33}. We will be mainly concerned with trajectories of the first type, and for them, $f^J_{00}(t) = f^J_{33}(t) = 0$.

The transition amplitudes given by Eq. (10) are defined for integer J values. Therefore, they will have to be analytically continued into the complex J plane to make them suitable for a Regge pole model. When this is done one obtains[4,8,11]

$$f_1 \approx \frac{t}{4m^2-t}\,\zeta g_{00}(t) z^{\alpha} \quad ,$$

$$f_2 \approx \zeta g_{11}(t) z^{\alpha} \quad , \tag{12}$$

$$f_3 \approx \frac{t}{4m^2-t}\left\{\zeta g_{33}(t)\left[\frac{d}{dz}(z^{\alpha}) + \frac{d^2}{dz^2}(z^{\alpha})\right] - \zeta g_{22}(t)\alpha \frac{d}{dz}(z^{\alpha-1})\right\} \quad ,$$

$$f_4 \approx \frac{t}{4m^2-t}\left\{\zeta g_{22}(t)\left[\frac{d}{dz}(z^{\alpha}) + \frac{d^2}{dz^2}(z^{\alpha})\right] - \zeta g_{33}(t)\alpha \frac{d}{dz}(z^{\alpha-1})\right\} \quad ,$$

$$f_5 \approx -\zeta g_{12}(t) \frac{d}{dZ}(Z^{\alpha}) \quad ,$$

where, in addition, the asymptotic behavior near $t = 0$ has been factored out and the Legendre polynomials have been replaced by their leading term. Some of the factors that appear in Eq. (10) have been absorbed into the functions $g_{00}(t)$, $g_{11}(t)$, $g_{22}(t)$, $g_{12}(t)$, and $g_{33}(t)$, which are the residue functions. The total angular momentum has gone into $\alpha(t)$, a complex function of t.

The factorization theorem, that is, Eq. (11), here has the equivalent form

$$g_{11}(L,t)g_{22}(L,t) = [g_{12}(L,t)]^2 \quad . \tag{13}$$

It is assumed that all the information regarding the real and imaginary part of the amplitude is contained in the signature factor ζ, which in Eqs. (4) and (12) has been factored out. This assumption has its origin in an analogy with potential scattering, in which, under certain conditions, it can be shown that the residue functions are real analytic functions.[12] If this assumption is valid, ζ_{iL} as defined by Eq. (4) is a scalar function of s and t.

For the trajectories for which we will be mostly concerned here -- that is, P, P', ω, ρ, and B -- Eq. (12) becomes

$$f_{1L} = 0 \quad ,$$

$$f_{2L} = \zeta_L \varepsilon_{11}(L,t) Z^{\alpha_L} ,$$

$$f_{3L} = -\frac{t}{4m^2-t} \zeta_L \varepsilon_{22}(L,t) \alpha_L(\alpha_L - 1) Z^{\alpha_L - 2} , \qquad (14)$$

$$f_{4L} = \frac{t}{4m^2-t} \zeta_L \varepsilon_{22}(L,t) \alpha_L^2 Z^{\alpha_L - 1} ,$$

$$f_{5L} = -\zeta_L \varepsilon_{12}(L,t) \alpha_L Z^{\alpha_L - 1} .$$

Up to now, we have given the prescription for obtaining σ_τ, $d\sigma/dt$, and P, provided that the trajectories and residue functions are known, but the case is that nothing is known about the residue functions for $t < 0$ and very little about the trajectories. But, there exist experimental data for p-p, $\bar{p}$-p, p-n, and $\bar{p}$-n total cross sections, for p-p and $\bar{p}$-p differential cross sections, and for p-p polarizations, and we will use these data to inquire phenomenologically into the functions $\alpha_L(t)$, $\varepsilon_{11}(L,t)$, and $\varepsilon_{22}(L,t)$. This will be done by assuming convenient parametric forms for these functions and taking sets of experimental points to minimize expressions of the type

$$\chi^2 = \left| \frac{\left[\sigma_t(s_1,t_1)\right]^{th} - \left[\sigma_t(s_1,t_1)\right]^{exp}}{\text{Error}\left[\sigma_t(s_1,t_1)\right]^{exp}} \right|^2 + \cdots + \left| \frac{\left[\sigma_t(s_n,t_n)\right]^{th} - \left[\sigma_t(s_n,t_n)\right]^{exp}}{\text{Error}\left[\sigma_t(s_n,t_n)\right]^{exp}} \right|^2$$

$$+ \left| \frac{\left[\frac{d\sigma}{dt}(s_1,t_1)\right]^{th} - \left[\frac{d\sigma}{dt}(s_1,t_1)\right]^{exp}}{\text{Error}\left[\frac{d\sigma}{dt}(s_1,t_1)\right]^{exp}} \right|^2 + \cdots + \left| \frac{\left[\frac{d\sigma}{dt}(s_m,t_m)\right]^{th} - \left[\frac{d\sigma}{dt}(s_m,t_m)\right]^{exp}}{\text{Error}\left[\frac{d\sigma}{dt}(s_m,t_m)\right]^{exp}} \right|^2$$

$$+ \left| \frac{\left[P(s_1,t_1)\right]^{th} - \left[P(s_1,t_1)\right]^{exp}}{\text{Error}\left[P(s_1,t_1)\right]^{exp}} \right|^2 + \cdots + \left| \frac{\left[P(s_\ell,t_\ell)\right]^{th} - \left[P(s_\ell,t_\ell)\right]^{exp}}{\text{Error}\left[P(s_\ell,t_\ell)\right]^{exp}} \right|^2$$

where the superscript th stands for the calculated value and the superscript exp for the corresponding experimental value. The minimization with respect to trial residue functions was carried out by the variable metric minimization method[13] and with respect to trial trajectories by the method Conser.[14]

The $\alpha(L,t)$ parametric forms adopted were straight lines and trajectories with curvature. At least near $t = 0$, the trajectories are expected to behave like straight lines with high slopes. In this way, they may pass through known particle poles and intercepts. The form most extensively investigated was

$$\alpha(L,t) = \alpha(L,0) + \alpha(L,1)t + \alpha(L,2)t^2 \quad , \tag{16}$$

where the parameters to be determined are the coefficients, except where already known from π-N scattering or from another source.

In order to preclude the existence of particles of negative mass, the residue must vanish for the momentum transfer for which the corresponding trajectory passes through a meaningful J value. This condition was imposed.

The parameterizations of the residue functions most extensively used were of the type

$$g_{11}(L,t) = \left[B(1,L)e^{B(2,L)t}\right]^2 + \frac{t}{4m^2-t}\left(\frac{4m^2-t_{0L}}{-t_{0L}}\right)\left[B(1,L)e^{B(2,L)t_{0L}}e^{B(4,L)(t-t_{0L})}\right]^2$$

$$g_{22}(L,t) = \left[G(1,L)e^{G(2,L)t}\right]^2 F[\alpha(L,t)] \qquad (17)$$

where $F[\alpha(L,t)] = [\alpha(L,t)]^2$ for trajectories of even signature and $F[\alpha(L,t)] = [\alpha(L,t) + 1]^2(0.12 + t)$ for trajectories of odd signature.

The adjustable parameters of $g_{11}(L,t)$ are $B(1,L)$, $B(2,L)$, and $B(4,L)$, and those of $g_{22}(L,t)$ are $G(1,L)$, and $G(2,L)$. The momentum transfer at which the $g_{11}(L,t)$ residue function is compelled to vanish is t_{0L}, which, for trajectories of even signature, is the t value at which the trajectory crosses the axis $\alpha(L,t) = 0$, and for trajectories of odd signature, is the t value at which the trajectory crosses the axis $\alpha(L,t) = -1$. The function $g_{22}(L,t)$ is made to vanish at these points by means of the factors $[\alpha(L,t)]^2$ and $[\alpha(L,t) + 1]^2$ for trajectories of even and odd signature respectively. The factor $(0.12 + t)$ is introduced to satisfy the condition of real analyticity of the residues of odd signature, since for these trajectories the function $g_{11}(L,t)$ becomes negative at $t \approx -0.12\ (\text{GeV})^2$. This will be seen in Section IV. The $g_{12}(L,t)$ functions vanish at the t_{0L} points by the factorization condition, Eq. (13).

B. Charge-Exchange Scattering

In charge exchange it is possible to have the contribution of trajectories of isospin 1 or greater, and of the trajectories that can be exchanged in the N-N case, ρ, R and π satisfy this requirement. It is known that π gives zero contribution in the forward direction,[4] and since it lies lower than ρ and R, it will be neglected.

The p-n and $\bar{p}$-n charge-exchange scattering amplitudes, $\Phi_i(\text{pn ch ex})$, and $\Phi_i(\bar{p}\text{n ch ex})$, are determined as follows. The amplitude $\Phi_i(\text{pn ch ex})$ is related by general isotopic spin agruments to the difference between the amplitudes for elastic p-p and p-n scattering in the form

$$\Phi_i(\text{pn ch ex}) = \Phi_i(0,2) - \Phi_i(1,2) \quad . \tag{18}$$

This equation is now written in terms of the individual trajectory contributions with the help of Eqs. (4) through (8), and in this form one obtains

$$\Phi_i(\text{pn ch ex}) = 4(2\alpha_\rho + 1)\zeta_\rho\phi_{i\rho}(1,2) + 4(2\alpha_R + 1)\zeta_R\phi_{iR}(1,2) \quad . \tag{19}$$

Now, taking into account G parity conservation, Eq. (9), and Eq. (19), one obtains the remaining amplitude, e.g.,

$$\Phi_i(\bar{p}\text{n ch ex}) = 4(\alpha\rho + 1)\zeta_\rho\phi_{i\rho}(1,2) - 4(2\alpha_R + 1)\zeta_R\phi_{iR}(1,2) \quad . \tag{20}$$

The total cross sections, differential cross sections, and polarizations for these processes can now be obtained by introducing these amplitudes in Eqs. (1), (2), and (3).

III. TOTAL CROSS SECTIONS AND RATIO OF THE REAL TO THE IMAGINARY PARTS OF THE AMPLITUDE

We soon realize the convenience of considering first in some detail the situation at zero momentum transfer. Here, the results are expected to be more important and meaningful; there is more experimental and theoretical information in the forward direction than for any other t value, and any conclusion depends, for each trajectory, only on the values of $\alpha(L,1)$ and $g_{11}(L,0)$.

The most accurate and abundant $t = 0$ data are the total cross sections. Hence, we have relied on this information to fix the parameters $\alpha(L,1)$ and $g_{11}(L,0)$. Then, we have used these values to evaluate forward direction quantities for which some data or deductions from experiment exist, such as $\frac{d\sigma}{dt}(t = 0)$ and the ratio of the real to the imaginary parts of the amplitude.

More emphasis has been put on the energy range above 6 GeV/c, where the Regge pole model can be applied with more confidence. For this reason, we have used the total cross section data in the energy range 6 to 22 GeV/c.[15]

The trajectories P, P', ω, ρ, R, and Φ are investigated in the forward direction. It is found that P, P', and ω are sufficient to account for $\sigma_t(pp)$ and $\sigma_t(\bar{p}p)$, and although the contributions of ρ and R are small, they are included to account for the $\sigma_t(pn) - \sigma_t(pp)$ and $\sigma_t(\bar{p}p) - \sigma_t(\bar{p}n)$ differences. The Φ trajectory has the same quantum numbers as ω, but it is expected to be of less importance because of its relative position in a Chew-

Frautschi diagram, where we have $\mathrm{Re}\alpha(\omega,m_\omega^2) = \mathrm{Re}\alpha(\phi,m_\phi^2)$, and $m_\phi > m_\omega$. Because of this, we expect to have $\alpha(\omega,0) > \alpha(\phi,0)$, and if in addition one assumes that

$$g_{11}(\omega,0) \geq g_{11}(\phi,0) \quad ,$$

one finds that the best fit to the data is obtained for $\alpha(\phi,0) \ll 0$ or $g_{11}(\phi,0) \approx 0$. Therefore, the ϕ contribution is neglected.

With the use of Eq. (1) and some of the relevant subsequent equations, the total cross sections can be written in terms of the trajectory contributions,

$$\begin{aligned}
\sigma_t(pp) &= \mathrm{Im}[A(P) + A(P') - A(\omega) - A(\rho) + A(R)] \quad , \\
\sigma_t(np) &= \mathrm{Im}[A(P) + A(P') - A(\omega) + 3A(\rho) - 3A(R)] \quad , \\
\sigma_t(\bar{p}p) &= \mathrm{Im}[A(P) + A(P') + A(\omega) + A(\rho) + A(R)] \quad , \\
\sigma_t(\bar{p}n) &= \mathrm{Im}[A(P) + A(P') + A(\omega) - 3A(\rho) - 3A(R)] \quad ,
\end{aligned} \tag{21}$$

where $\mathrm{Im}A(L)$ gives the L trajectory contribution. The corresponding plus or minus signs of these contributions are shown explicitly.

The $\sigma_t(pn) - \sigma_t(pp)$ and $\sigma_t(\bar{p}p) - \sigma_t(\bar{p}n)$ differences depend on ρ and R , according to

$$\begin{aligned}
\sigma_t(pn) - \sigma_t(pp) &= \mathrm{Im}[4A(\rho) - 4A(R)] \quad , \\
\sigma_t(\bar{p}p) - \sigma_t(\bar{p}n) &= \mathrm{Im}[4A(\rho) + 4A(R)] \quad .
\end{aligned} \tag{22}$$

It is known from experiment that these differences are small in the energy range under consideration, and from this, one concludes that the ρ and R contributions are small compared with those of P , P' , and ω , which have to account for the large values of $\sigma_t(\bar{p}p)$, $\sigma_t(pp)$, and $\sigma_t(\bar{p}p) - \sigma_t(pp)$.

The forward direction ρ and R parameters are subject to various constraints, e.g., (a) they have to satisfy simultaneously Eqs. (19), (20), and (22); (b) the ρ trajectory alone dominates the high energy process $\pi^- + p \to \pi^\circ + n$, from which the ρ trajectory has been determined;[16] (c) similarly, the R trajectory dominates the process $\pi^- + p \to \eta^\circ + n$, from which the R trajectory has been determined.[17] Therefore, provided that ρ and R are indeed the main contributors to the processes just mentioned, the ρ and R parameters at $t = 0$ could be determined from a simultaneous fit to p-n and $\bar{p}$-n charge-exchange scattering, and to the $\sigma_t(\bar{p}p)$ $-\sigma_t(\bar{p}n)$ and $\sigma_t(pn) - \sigma_t(pp)$ differences, with trajectory intercepts in agreement with (b) and (c) above. From the foregoing discussion one concludes that the ρ and R parameters in the forward direction may be determined uniquely. However, the existing experimental data are subject to large errors, in particular the $\sigma_t(\bar{p}n)$ and $\bar{p}$-n charge-exchange data. Accurate determination of these data would allow a test of the ρ and R model, for which the relations

$$\sigma_t(\bar{p}p) - \sigma_t(\bar{p}n) > \sigma_t(pn) - \sigma_t(pp)$$

$$\sigma_t(\bar{p}n \text{ ch ex}) > \sigma_t(pn \text{ ch ex}) \qquad (23)$$

at corresponding energy are always valid.

The $\sigma_t(pn) - \sigma_t(pp)$ difference is known more accurately.[15,18] The same is true of the p-n charge-exchange data.[19,20] Therefore, to determine the ρ and R residues we use the data of Refs. 15 and 20, and the intercepts found from Refs. 16 and 17. These determinations are then tested by calculating the remaining $t = 0$ quantities and comparing them with existing experimental data. The ρ and R contributions determined in this form are included as minor adjustments in $\bar{p}$-p and p-p scattering.

The p-p and $\bar{p}$-p cross sections require at least three main contributors, the P trajectory to account for the asymptotic limit of the total cross sections, ω to account for the $\sigma_t(\bar{p}p) - \sigma_t(pp)$ difference, and P' to explain the flatness of $\sigma_t(pp)$, by cancellation with the ω contribution. Here we have three trajectories but there exist more accurate and numerous data than for p-n and $\bar{p}$-n charge exchange. Also, two of the trajectory intercepts are known. The P intercept can be taken at the Froissart limit,[21] and the P' as found in π-N calculations.[22] Next, with the use of this model, we estimate the value of the ω intercept.

The small number of data points and their relatively large errors do not allow a unique determination of the residues and the ω intercept. Nevertheless, we find that a good fit is obtained when the residues are similar in value and the intercept is near the expected value in the Chew-Frautschi diagram. Therefore, as a first step in the determination of the ω intercept, we may assume that the $t = 0$

residues of P , P' , and ω are equal, e.g.,

$$g = g_{11}(P,0) \approx g_{11}(P',0) \approx g_{11}(\omega,0) \quad . \tag{24}$$

If various trial values of the coupling, g , are assumed, and the best ω intercept, $\alpha(\omega,1)$, is found, one obtains the results shown in Fig. 1. Here we plot the χ^2 per point and the best ω intercept vs g . The best fit is obtained when $g \approx (2.64)^2$ and $\alpha(\omega,1) \approx 0.5$. Using this value for the ω intercept and relaxing the condition of Eq. (24), we find that the best fit is obtained when $g_{11}(P,0) \approx (2.48)^2$, $g_{11}(P',0) \approx (3.05)^2$, and $g_{11}(\omega,0) \approx (2.70)^2$, with a χ^2 per point equal to 0.13 for the $\bar{p}$-p and p-p of data of Ref. 15. In both cases the existing data are well satisfied.

The results just obtained remain essentially unchanged when the ρ and R contributions are included. The parameters corresponding to these contributions are obtained from a fit to the 17-$(\text{GeV})^2$ p-n charge-exchange data[20], which are found to be in agreement with the p-p , p-n , $\bar{p}$-p , and $\bar{p}$-n data of Ref. 15. The values obtained are $g_{11}(\rho,0) \approx (0.54)^2$ and $g_{11}(R,0) \approx (0.78)^2$.

In Fig. 2, we show the results obtained under the assumption of equal P , P' , and ω couplings. In this case the χ^2 per point is equal to 0.7 for the p-p , $\bar{p}$-p , p-n , and $\bar{p}$-n data of Ref. 15. The calculated p-p and $\bar{p}$-p total cross sections with different P , P' , and ω couplings are shown in Fig. 3.

The following conclusions may be derived. The p-p and $\bar{p}$-p total cross sections above 10 $(GeV)^2$ are reproduced very well by a Regge model that includes the trajectories P , P' , and ω . The results show that the present experimental high energy is outside the validity of the asymptotic one-pole approximation.

In the low-energy range, all the calculated cross sections tend to increase rapidly below 10 $(GeV)^2$. This contradicts the behavior of experimental $\sigma_t(pn)$, which, on the contrary, tends to decrease at 9 $(GeV)^2$.[18,23] Also the experimental $\sigma_t(pp)$ begins to show structure below 9 $(GeV)^2$.[18] Our results are not in agreement with an earlier fit of the $\sigma_t(pn) - \sigma_t(pp)$ difference,[24] which was made without the $\sigma_t(pn)$ and $\sigma_t(\bar{p}n)$ data, which are now available. The inapplicability of the Regge model in the low-energy region is not strange, since here the singularities of the direct channel may be important, and apparently this is the case in p-p and p-n scattering. The $\sigma_t(\bar{p}p) - \sigma_t(\bar{p}n)$ difference seems in disagreement with the ρ and R model, but the $\bar{p}$-n data are subject to very large errors and hence it is difficult to arrive at a definite conclusion.

The calculated cross sections in the high-energy range provide an estimate of the proximity to the asymptotic limit. This is shown in Table IV, where it can be seen that much higher energies are required to approach this limit.

Experimental determinations have been made of the ratio of the real to the imaginary parts of the amplitude, $R = Re(\Phi_1 + \Phi_3)/Im(\Phi_1 + \Phi_3)$, for some R(pp) points[25] and one R(pn) point.[26] With

the parameters $g \approx (2.64)^2$ and $\alpha(\omega,1) \approx 0.5$ found first, we have calculated these ratios. The results, shown in Fig. 4, are in good agreement with experiment, which indicates that $R(pp)^{exp} \approx -0.3 \pm 0.1$. There are no experimental $R(\bar{p}p)$ and $R(\bar{p}n)$ determinations. Here, our calculated ratios indicate that the $\bar{p}$-p and $\bar{p}$-n amplitudes in the forward direction are almost pure imaginary because of an almost complete cancellation of the P' contribution to the real part by ω. This is in contrast to the p-p and p-n amplitudes in the forward direction, where there is an almost complete cancellation of the P' contribution to the imaginary part by ω. Our conclusions are at variance with a recent work,[27] which predicts a larger percentage of the real part for $R(\bar{p}p)$ and $R(\bar{p}n)$.

With the same parameters, $g \approx (2.64)^2$ and $\alpha(\omega,1) \approx 0.5$, we have calculated p-n and $\bar{p}$-n differential cross sections in the forward direction, shown in Fig. 5. The p-p and $\bar{p}$-p cases shown by dashed lines correspond to calculations exclusive of the Coulomb interaction. Extrapolations of experimental differential cross sections seem in agreement with these results.

IV. DIFFERENTIAL CROSS SECTIONS AND POLARIZATIONS

Because of the asymptotic conditions in the forward direction, the contribution of the $g_{22}(t)$ residue functions is zero in this direction. This can be seen in Eq. (14), where the asymptotic behavior is explicitly factored out in each of the amplitudes. Consequently, the same is true of the residue function $g_{12}(t)$, because of the factorization condition, Eq. (13). Nevertheless, at the region $t < 0$, all the residue functions may be different from zero and all must be taken into account.

The fact that the residue functions, $g_{22}(t)$ and $g_{12}(t)$, contribute for $t < 0$ complicates the calculations considerably, because then it is necessary to include the complete spin structure of the amplitudes.[28] The physical constraints of unitarity, factorization, and the assumption of real analyticity of the residues continue to hold as for Section III. Therefore, while fitting the data, we enjoy no more freedom in this region unless one relaxes one or more of the physical constraints, in which case the data may be satisfied in various ways.

In the case $t = 0$, we relied on the most abundant data, e.g., total cross sections, to obtain information on $g_{11}(t = 0)$. We used the optical theorem and the fact that in the Regge pole theory all the information regarding the real and imaginary parts of the amplitude is contained in the signature factors, which are known. For this reason, we were able to calculate immediately $\frac{d\sigma}{dt}(t = 0)$ and $R(t = 0) = \mathrm{Re}(\phi_1 + \phi_3)/\mathrm{Im}(\phi_1 + \phi_3)$.

For $t < 0$, we rely on $d\sigma/dt$ and P to obtain information on the trajectories and on $g_{11}(t)$ and $g_{22}(t)$; $g_{12}(t)$ is obtained by means of the factorization condition, Eq. (13). In the region $-1.0 < t < 0$, $d\sigma/dt$ has a constant slope when plotted vs t on a semilogarithmic scale. The slopes of $\bar{p}$-p and p-p are very different, about 15 and 6.6 respectively.[29] In addition, they intersect at an invariant moment transfer of about $-0.15\ (GeV)^2$. This information is found to be of importance in the determination of the behavior of the residue functions.

Fitting the data, one finds that the function $g_{11}^{1}(t)$ is most important, since the fit depends strongly on its form. On the other hand $g_{22}(t)$ is found to be relevant to phenomena such as polarization, which is high at low energies and becomes negligible as the energy increases.

The physical condition that the $g_{11}(t)$ residue must vanish for the momentum transfer for which the corresponding trajectory passes through a physically meaningful J value has been imposed, at precisely that value of t, by cancellation of the two terms of Eq. (17). That is, the vanishing of the $g_{11}(t)$ residue is not accomplished, as it is usually done, by means of either the factor α or $\alpha + 1$. In this form we avoid constraining the behavior of this residue when a trial trajectory is chosen asymptotic to the axis $\alpha = 0$. The vanishing of $g_{22}(t)$ in these points is accomplished by the factors α^2 or $(\alpha + 1)^2$ according to whether the trajectory is of even or odd signature.

The determination of the parameters of Eqs. (16) and (17) is made as indicated in Section II. We use the p-p and $\bar{p}$-p differential

cross-section data of Ref. 29, and the p-p polarization data of Ref. 30. The calculations are restricted to energies in the interval 10 to 50 $(GeV)^2$ and to momentum transfers in the interval 0 to -1.0 $(GeV)^2$.

Similarly as for $t = 0$, the p-p and $\bar{p}$-p scattering is essentially controlled by P, P', and ω. The ρ and R contributions are, in comparison, small. Therefore the p-p and $\bar{p}$-p data are studied with P, P', and ω only.

We have noticed after numerous trial calculations that the best fits to the data are consistent with the assumption of straight-line trajectories, or trajectories with small curvature. In the same form, we find that the physical constraints that we have imposed are very strong, in a sense that if we consider acceptable solutions only those with a reasonable χ^2, then the parameters may vary only within narrow limits. Within this criterion, we find that for straight-line trajectories, the slopes are confined to the intervals $0.25(GeV)^{-2} < \alpha'(P) < 0.4(GeV)^{-2}$, $1.1(GeV)^{-2} < \alpha'(P') < 1.4(GeV)^{-2}$, and $0.7(GeV)^{-2} < \alpha'(\omega) < 0.9(GeV)^{-2}$. In Fig. 6 we show a set of straight-line trajectories for which we find good agreement. The particles with which they are possibly associated are also shown. Inspection of this figure indicates a clear association of the ω trajectory with the $\omega(783)$ particle-pole. There is also a very likely association of the P' trajectory with either the particle pole $f_0(1250)$ or $f'(1525)$. The association of the P trajectory of Fig. 6 with $f_0(1250)$ seems less plausible, since the trajectory slopes are expected to decrease eventually in this region. Nevertheless, this is

not a real impediment, since the trajectory could first increase, then after reaching the particle, decrease.

For each set of trajectories, there is a set of residue functions that give the best fit. In this form, for the trajectories of Fig. 6, we find the residue functions specified by the parameters of Table V, also depicted graphically in Figs. 7 and 8. For this particular calculation, we obtain a χ^2 per point of 1.5 for the data of Refs. 29 and 30.

We would like to note at this point that the $d\sigma/dt$ and P data available are not very accurate and that there are not enough statistics. Therefore, one should not consider the solution given by Figs. 6, 7, and 8 as unique, but as one that typifies the behavior of trajectories and residue functions.[31] Besides, the model used in this interpretation is a simple one, which neglects all the low-lying trajectories. The slight intrusion of the $g_{11}(P',t)$ residues of P' into the negative side of the plane, is interpreted as fictitious and due to the simplicity of the model.

With the parameters given above, we have calculated the p-p and $\bar{p}$-p differential cross sections shown in Fig. 9. We notice that the calculated $\bar{p}$-p differential cross sections show almost no shrinkage as compared with p-p. These characteristics are in agreement with the experiments. In this model, the negligible $\bar{p}$-p shrinkage, notably for $t < -0.3$ $(GeV)^2$, seems connected to the following circumstances. The residue $g_{11}(P',t)$ of P' is very small in this region, and there are appropriate cancellations and compensations between the P and ω contributions to the real and imaginary parts of

the amplitude at different energies. The P' trajectory crosses the axis, $\alpha = 0$, near $t = -0.6$ (GeV)^2.

The slope of the calculated $\bar{p}$-p differential cross sections shown in Fig. 9 seems smaller than the experimental slope. This can be attributed to the limitations of the model. In particular, the parametrization of the $g_{11}(t)$ residues, by means of a difference of exponentials, is inadequate to cover well the interval $0 < t < -1.0$ (GeV)^2. For the set of trajectories of this sample calculation a higher slope can be easily obtained but with a slightly χ^2 per point. In the particular fit shown in Fig. 9, less importance is given to the $\bar{p}$-p data by fitting only a few of these points.

The calculated p-p polarizations are shown in Fig. 10. The slight depressions around $t = -0.35$ (GeV)^2 seem to be fictitious, due to the limitations of the model. The calculated $\bar{p}$-p polarizations at 10 (GeV)^2 constitute a prediction of the model. They indicate that the $\bar{p}$-p polarizations are about equal in magnitude and form to those of p-p but of opposite sign, e.g., the scattered particles tend to become oriented in opposite directions.

Experimental information has been collected on the relation of maximum angular p-p polarization, P_{max}, which takes place around $t \approx -0.25$ (GeV)^2, and the invariant energies.[30,32] In Fig. 11, we show the P_{max} values calculated with the present model. Comparison with experiment indicates that the Regge model gives the correct behavior, except perhaps that the tail of P_{max} calculated is higher because of the trajectories neglected.

V. THE p-n AND $\bar{p}$-n CHARGE-EXCHANGE SCATTERING AT SMALL ANGLES

The slope of the p-n charge-exchange differential cross section is unusually high in the interval of momentum transfers 0 to -0.05 $(\text{GeV})^2$, then becomes of about the same magnitude as that of p-p.[19,20] By use of the data of Ref. 19, it has been shown[33] that these features can be reproduced by a ρ' and R model of the following characteristics: a ρ trajectory of high intercept and large slope; an R trajectory of low intercept and small slope; a fast-decreasing ρ residue, $g_{11}(\rho,t)$; and a slow-decreasing R residue, $g_{11}(R,t)$. This simple interpretation is in agreement with the ρ and R trajectory determinations from π-N scattering,[16,17] the apparent s independence of the p-n charge-exchange slope at small angles, and the comparatively small $\bar{p}$-n charge-exchange slope.[34]

We use this procedure and the trajectories $\alpha(\rho,t) = 0.6 + 0.8t$ and $\alpha(R,t) = 0.35 + 0.35t$ to fit the 8.0-GeV/c data of Ref. 20. The results are shown in Fig. 12. The data points are not included because they are very numerous, but the χ^2 of 0.94 obtained is proof of a good fit. The method followed works as well at 8.0 GeV/c as at 3.0 GeV/c.[33] The parameterizations obtained here are slightly different from those obtained at the lower energy, but the general behavior of the residue functions still prevails. The singularities of the direct channel and systematic errors of the experimental measurements may be cited as possible causes. The discrepancy is noticed also at zero momentum transfer, where the π trajectory, which was ignored, does not contribute.[4]

We show also, in Fig. 12, calculated $\bar{p}$-n charge-exchange differential cross sections at $s = 20\ (GeV)^2$. The slope near the forward direction is small, as it is at $7.5\ (GeV)^2$.

The residue functions obtained are shown in Figs. 13 and 14. They are equivalently given by Eq. (17) and the parameters of Table VI. Of these, $B(1,\rho)$ and $B(1,R)$ are used in Section III in the calculations of total cross sections. They give a smaller $\sigma_t(\bar{p}p) - \sigma_t(\bar{p}n)$ difference than those obtained from a fit to the 3.0-GeV/c data, and for this reason, they are preferred. The residue functions obtained from this fit have more meaning near the forward direction, where the $g_{22}(t)$ residues do not contribute. For $t \leq -0.1\ (GeV)^2$ the data may be satisfied in various ways according to the values that $g_{11}(\rho,t)$, $g_{11}(R,t)$, $g_{22}(\rho,t)$, and $g_{22}(R,t)$ may have. Here we do not have polarization data in addition to $d\sigma/dt$ to restrict this freedom. Therefore, the form of the residues obtained for $t \leq -0.1\ (GeV)^2$ may not be very meaningful. Nevertheless, there is indication that the residue functions $g_{22}(\rho,t)$ and $g_{22}(R,t)$ may be large, as indicated by the large value that the $g_{22}(\rho,t)$ residue obtains. These two residues are associated with the spin-flip term in π-N scattering, the $g_{22}(\rho,t)$ residue in $\pi^- + p \to \pi^0 + n$, and the $g_{22}(R,t)$ in $\pi^- + p \to \eta^0 + n$. Here also there is evidence that these residues are large,[35] and that the residue $g_{11}(\rho,t)$ becomes negative for small momentum transfers. In N-N scattering, because of the assumption of real analyticity of the residues, when $g_{11}(\rho,t)$ changes sign, so also does $g_{22}(t)$. Since this happens at about $t = -0.1\ (GeV)^2$, the asymptotic condition and this statement imply that

$g_{22}(\rho,t)$ must be small in the t interval 0 to -0.1 $(GeV)^2$. This fact is in agreement with the residue functions found for ρ and with the mechanism used to describe p-n charge exchange at small angles.

It is possible that the π trajectory may have an important contribution at momentum transfers of the order $t \approx -0.5\ (GeV)^2$, and this may be connected with the fact that, when the data are fitted, $g_{22}(\rho,t)$ becomes very large at about these momentum transfers.

The $g_{22}(R,t)$ residue, according to π-N scattering, is large.[35] This is at variance with the result found here. There is the possibility that some cancellation with the ρ contribution or other trajectory may take place.

VI. CONCLUSIONS

The method used[4-8,10,12] takes into account unitarity, the complete spin structure, and the factorization and real analyticity of the residues. It is a method in which only simple pole trajectories in the crossed channel are considered. It does not consider singularities of the direct channel nor possible branch cuts.

The trajectories P, P', ω, ρ, and R are used to account for existing experimental data, which includes total cross sections, differential cross sections, polarizations, and ratio of the real to the imaginary parts of the amplitude. Good agreement is obtained for processes in which P, P', and ω are the main contributors, and apparently poor agreement at low energies for processes in which ρ and R are the main contributors. Nevertheless, the $\bar{p}$-n elastic and $\bar{p}$-n charge-exchange data are scanty and subject to large errors. More accurate measurements of them will decide whether the ρ and R model used to describe them here is adequate. There is consistency between the model and all the existing data if the lower energies, $s \leq 10\ (\mathrm{GeV})^2$, are excluded.

When fitting the data, one finds that the physical constraints mentioned above are very restrictive, and if, for example, the assumption of real analyticity of the residues is ignored, the data may be satisfied more freely. It is the full use of the constraints that permits the specification of the behavior of residues and trajectories given here.

ACKNOWLEDGMENTS

The author is indebted to Dr. William Rarita for introducing him to the study of the N-N problem and for continued encouragement, to Professor Geoffrey F. Chew for encouragement and advice, to Dr. Naren F. Bali for useful comments, to Mr. Thomas Clements for programming assistance. He thanks Professor Burton J. Moyer and Dr. David L. Judd for the hospitality of the Physics Department and Lawrence Radiation Laboratory, University of California, Berkeley, respectively.

Table I. Trajectories assumed most important in high-energy N-N scattering.

Trajectory Name	Designation (L)	Possible Association With the Nonet 2^+	Possible Association With the Nonet 1^-	J Parity	I'
Pomeranchuk	P	$f_o(1250)$?		even	0
Igi	P'	f'(1525)		even	0
ω	ω		$\omega(783)$	odd	0
ρ	ρ		$\rho(760)$	odd	1
Pignotti	R	$A_2(1300)$		even	1

Table II. Partial transition amplitudes between the $\overline{N}$-N states of the crossed t channel.

	Singlet (s = 0)	Triplet (s = 1)		
	$P_\tau = -1$	$P_\tau = +1$		$P_\tau = -1$
	$J = L$	$J = L \pm 1$		$J = L$
State	0	1	2	3
0	$f^J_{00}(t)$			
1		$f^J_{11}(t)$	$f^J_{12}(t)$	
2		$f^J_{21}(t)$	$f^J_{22}(t)$	
3				$f^J_{33}(t)$

Table III. Quantum numbers of known trajectories that communicate with the $\bar{N}$-N crossed channel.

Trajectory Name	$P\tau$	S	τ	P	I'	G
P,P'	+	1	+	+	0	+
ω,ϕ	+	1	-	-	0	-
ρ	+	1	-	-	1	+
R	+	1	+	+	1	-
π	-	0	+	-	1	-
η,X^{o}	-	0	+	-	0	+
A_1	-	1	-	+	0	+

Table IV. Estimate of the maximum contribution of other than the Pomeranchuk trajectories at high energy N-N scattering.

Estimate (%)	14	8	6	5
s [in $(GeV)^2$]	100	400	600	1000

Table V. Best set of parameters of the P, P', and ω residue functions found for the trajectories of Fig. 6 and the p-p and $\bar{p}$-p dσ/dt and P data of Refs. 29 and 30.

Trajectory L	Parameters of the residue functions of P, P', and ω				
	B(1,L)*	B(2,L) [(GeV)$^{-2}$]	B(4,L) [(GeV)$^{-2}$]	G(1,L)	G(2,L) [(GeV)$^{-2}$]
P	2.48	1.15	1.24	5.14	1.37
P	3.05	1.03	2.04	29.61	1.00
ω	2.70	0.49	1.11	11.24	5.91

*The t = 0 parameters are found in Section III.

Table VI. The parameters of the ρ and R residue functions found for the data of Ref. 20 with the assumption of $\alpha(\rho,t) = 0.6 + 0.87t$ and $\alpha(R,t) = 0.35 + 0.35t$.

Trajectory L	Parameters of the residue functions of ρ and R				
	B(1,L)	B(2,L) [(GeV)^2]	B(4,L) [(GeV)^2]	G(1,L)	G(2,L) [(GeV)^2]
ρ	0.54	20.82	21.86	1.94	-5.37
R	0.78	1.66	0.64	0.16	8.19

FOOTNOTES AND REFERENCES

* Work performed under the auspices of the U.S. Atomic Energy Commission.

† Leave of absence from Instituto Politécnico Nacional and Comisión Nacional de la Energía Nuclear of México.

1. References on the S-Matrix Theory may be found in the monograph by G. F. Chew, The Analytic S-Matrix: A Basis for Nuclear Democracy (W. A. Benjamin and Co., 1966).

2. M. Froissart, in the Proceedings of the La Jolla Conference on Weak and Strong Interactions, unpublished report, 1961. V. N. Gribov, Zh. Eksperim. i Teor. Fiz. 41, 677 and 1962 (1961) [English translations: Soviet Phys. -- JETP 14, 478 and 1395 (1962)].

3. G. F. Chew and S. Frautschi, Phys. Rev. Letters 7, 394 (1961) and 8, 41 (1962).

4. I. J. Muzinich, Phys. Rev. 130, 1571 (1963).

5. I. J. Muzinich, Phys. Rev. Letters 9, 475 (1962).

6. A. Ahmadzadeh and E. Leader, Phys. Rev. 134, B1058 (1964).

7. M. L. Goldberger, M. T. Grisaru, S. W. MacDowell, and D. Y. Wong, Phys. Rev. 120, 2250 (1960).

8. D. H. Sharp and W. G. Wagner, Phys. Rev. 131, 2226 (1963).

9. V. B. Berestetskii, Zh. Eksperim. i Teor. Fiz. 44, 1603 (1963) [English translation: Soviet Phys. -- JETP 17, 1079 (1963)].

10. M. Gell-Mann, Phys. Rev. Letters 8, 142 (1962); V. N. Gribov and I. Ya. Pomeranchuk, Zh. Eksperim. i Teor. Fiz. 42, 1141 (1962) [English translation: Soviet Phys. -- JETP 15, 788 (1962)].

11. S. C. Frautschi, M. Gell-Mann, and F. Zachariasen, Phys. Rev. 126, 2204 (1962).

12. A. O. Barut and D. E. Zwanziger, Phys. Rev. 127, 974 (1962).

13. W. C. Davidon, Variable Metric Minimization Method, Argonne National Laboratory Report ANL-5990 (Rev.), 1959.

14. E. Beals, Lawrence Radiation Laboratory Computer Library Report ZO BKY Conser, 1965.

15. W. Galbraith, E. W. Jenkins, T. F. Kycia, B. A. Leontic, R. H. Phillips, A. L. Read, and R. Rubinstein, Phys. Rev. 138, B913 (1965).

16. G. Höhler, J. Baacke, H. Schlaile, and P. Sonderegger, Phys. Letters 20, 79 (1966).

17. R. J. N. Phillips and W. Rarita, Phys. Letters 19, 598 (1965).

18. R. F. George, K. F. Riley, R. J. Tapper, D. V. Bugg, D. C. Salter, and G. H. Stafford, Phys. Rev. Letters 15, 214 (1965).

19. J. L. Friedes, H. Palevsky, R. L. Stearns, and R. J. Sutter, Phys. Rev. Letters 15, 38 (1965).

20. G. Manning, A. G. Parham, J. D. Jafar, H. B. van der Raay, D. H. Reading, D. G. Ryan, B. D. Jones, J. Malos, and N. H. Lipman, Nuovo Cimento 41, A167 (1966).

21. M. Froissart, Phys. Rev. 123, 1053 (1961).

22. J. J. G. Scanio (Lawrence Radiation Laboratory), unpublished calculations, 1966.

23. A. N. Diddens, E. Lillethun, G. Manning, A. E. Taylor, T. G. Walker, and A. M. Wetherell, Phys. Rev. Letters 9, 32 (1962).

24. A. Ahmadzadeh, Phys. Rev. 134, B633 (1964).

25. L. F. Kirillova, V. Nikitin, V. Pantuev, V. Sviridov, L. Strunov, M. Khachaturyan, L. Khristov, M. Shaframova, Z. Korbel, L. Rob, S. Damyanov, A. Zlateva, Z. Zlatanov, V. Jordanov, Kh. Kanazirsky, P. Markov, T. Todorov, Kh. Chernev, N. Dalkhazhav, and D. Tuvdendorzh, Yadern. Fiz 3, 533 (1963) [translations: Soviet J. Nucl. Phys. 1, 379 (1965)]; A. E. Taylor, A. Ashmore, W. S. Chapman, D. F. Falla, W. H. Range, D. B. Scott, A. Astbury, F. Capocci, and J. G. Walker, Phys. Letters 14, 54 (1965); K. J. Foley, R. S. Gilmore, R. S. Jones, S. J. Lindenbaum, W. A. Love, S. Ozaki, E. H. Willen, R. Yamada, and L. C. L. Yuan, Phys. Rev. Letters 14, 74 (1965); G. Bellettini, G. Cocconi, A. N. Diddens, E. Lillethun, J. P. Scanlon, and A. M. Wetherell, Phys. Letters 19, 705 (1966).

26. G. Bellettini, G. Cocconi, A. N. Diddens, E. Lillethun, G. Matthiae, J. P. Scanlon, and A. M. Wetherell, Phys. Letters 19, 341 (1965).

27. V. Barger and M. Olsson, Phys. Rev. Letters 16, 545 (1966).

28. Unpublished calculations by the author indicate important discrepancies between formulations based on the complete spin structure and on the two-amplitude approximation, at least at the lower energy range.

29. K. J. Foley, R. S. Gilmore, S. J. Lindenbaum, W. A. Love, S. Ozaki, E. H. Willen, R. Yamada, and L. C. L. Yuan, Phys. Rev. Letters 15, 45 (1965).

30. H. M. Steiner, F. W. Betz, O. Chamberlain, B. D. Dieterle, P. D. Grannis, C. H. Shultz, G. Shapiro, L. V. Rossum, and D. M. Weldon, Polarization in Proton-Proton Scattering Using a Polarized Target, Lawrence Radiation Laboratory Report UCRL-11440, June 1964 (unpublished).

31. V. Flores-Maldonado, High-Energy $\overline{p}p$ and pp Differential Cross Sections and Residue Functions from Regge Poles, Lawrence Radiation Laboratory Report UCRL-16873, May 1966 (submitted to Phys. Letters).

32. V. P. Kanavetz, I. I. Levintov, B. V. Morozov, and M. D. Shafranov, Phys. Letters 7, 165 (1963).

33. V. Flores-Maldonado, Regge Pole Theory and p-n and $\overline{p}$-n Charge-Exchange Scattering at Small Angles, Lawrence Radiation Laboratory Report UCRL-16799, April 1966 (submitted to Phys. Rev. Letters).

34. O. Czyzwski, B. Escoubes, Y. Goldschmidt-Clermont, M. Guinea-Moorhead, D. R. O. Morrison, and S. De Unamuno-Escoubes, Phys. Letters 20, 554 (1966).

35. We are grateful to Professor Geoffrey F. Chew for bringing this point to our attention. The references are: R. J. N. Phillips and W. Rarita, Phys. Rev. 139, B1336 (1965); and Phys. Rev. Letters 15, 807 (1965), for the ρ and R processes respectively.

FIGURE CAPTIONS

Fig. 1. Determination of the ω intercept. Graph of $\alpha(\omega,1)$ and χ^2/point vs the coupling g, for the data of Ref. 15.

Fig. 2. Calculated N-N total cross sections as function of the invariant energy squared s (with the assumption of equal P, P', and ω couplings, and $\alpha(\omega,1) = 0.5$). Data from Ref. 15: ● p-p ; □ p-n ; o $\bar{p}$-n ; ▣ $\bar{p}$-p .

Fig. 3. Calculated $\bar{p}$-p and p-p total cross sections [with $g_{11}(P,0) \approx (2.48)^2$, $g_{11}(P',0) \approx (3.05)^2$, $g_{11}(\omega,0) \approx (2.70)^2$, and $\alpha(\omega,1) = 0.5$]. Data from Ref. 15: ● p-p ; ▣ $\bar{p}$-p .

Fig. 4. Ratio of the real to the imaginary parts of the amplitude in the forward direction as function of the invariant energy squared, s. Data from Refs. 25 and 26: ▣ p-p Kirillova et al.; □ p-p Foley et al.; ◇ p-p Taylor et al.; o p-p , ◈ p-n Bellettini et al.

Fig. 5. N-N differential cross sections in the forward direction as function of the invariant energy squared s. The p-p and $\bar{p}$-p calculations are exclusive of the Coulomb interaction.

Fig. 6. Straight-line trajectories, $\alpha(P,t) = 1.0 + 0.3t$, $\alpha(P',t) = 0.7 + 1.25t$, and $\alpha(\omega,t) = 0.5 + 0.7t$, used in the calculations shown in Figs. 9 and 10. The dashed lines are illustrative extrapolations.

Fig. 7. The $g_{11}(t)$ residue functions of P, P', and ω found for the trajectories of Fig. 6.

Fig. 8. The $g_{22}(t)$ residue functions of P, P', and ω found for the trajectories of Fig. 6 (with the threshold behavior included).

Fig. 9. Calculated p-p and $\bar{p}$-p differential cross sections as function of the invariant momentum transfer t. Data from Ref. 29.

- o p-p at $s = 22.36\ (\text{GeV})^2$;
- □ p-p at $s = 29.83\ (\text{GeV})^2$;
- ⊙ p-p at $s = 39.03\ (\text{GeV})^2$;
- ▣ p-p at $s = 42.85\ (\text{GeV})^2$;
- ◇ p-p at $s = 48.01\ (\text{GeV})^2$;
- Δ $\bar{p}$-p at $s = 23.97\ (\text{GeV})^2$;
- ▲ $\bar{p}$-p at $s = 31.67\ (\text{GeV})^2$.

Fig. 10. Calculated p-p polarizations at $s = 11.08$, 13.00, and $15.06\ (\text{GeV})^2$, as function of the invariant momentum transfer t. Data from Ref. 30:

- o at $s = 11.08\ (\text{GeV})^2$;
- □ at $s = 13.00\ (\text{GeV})^2$;
- ⊙ at $s = 15.06\ (\text{GeV})^2$.

The dashed line represents calculated $\bar{p}$-p polarizations, with this model, at $s = 10\ (\text{GeV})^2$.

Fig. 11. Calculated maximum angular polarizations, P_{max}, as function of the invariant energy squared.

Fig. 12. The p-n charge-exchange fit to the data of Ref. 20 at $s = 17\ (\text{GeV})^2$ and calculated $\bar{p}$-n charge-exchange differential cross sections at $s = 20\ (\text{GeV})^2$.

Fig. 13. The $g_{11}(t)$ residue functions of ρ and R, obtained from a fit to the data of Ref. 20.

Fig. 14. The $g_{22}(t)$ residue functions of ρ and R (with the threshold behavior included) obtained from a fit to the data of Ref. 20.

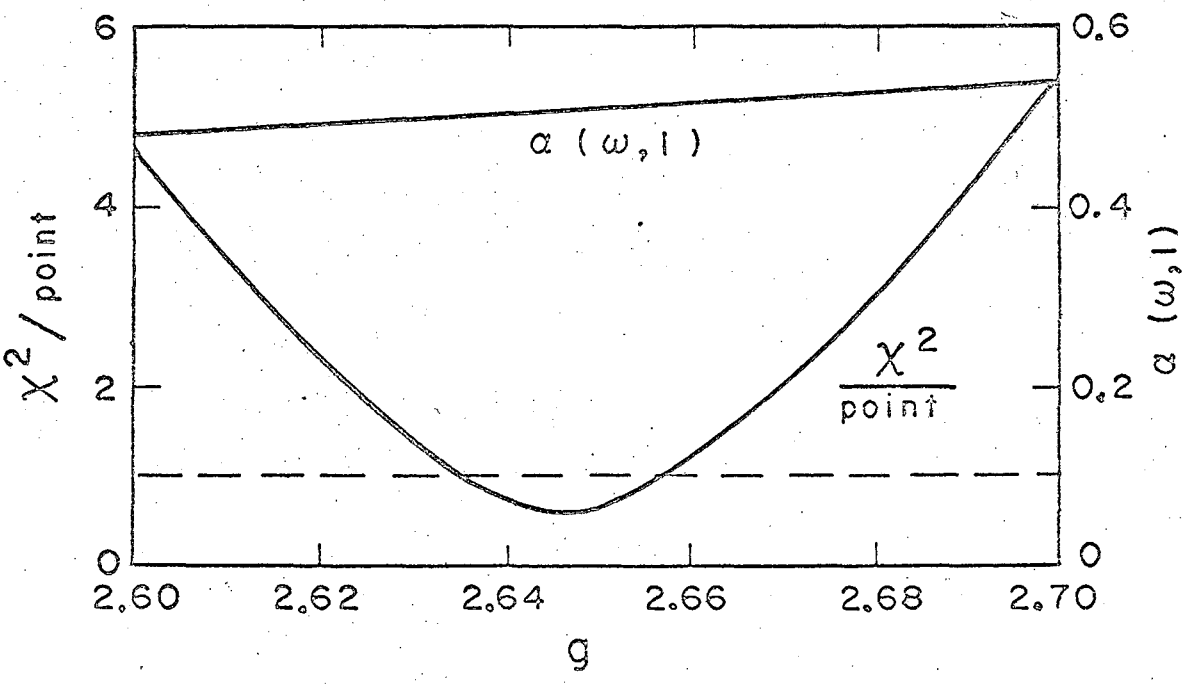

MUB-11361

Fig. 1

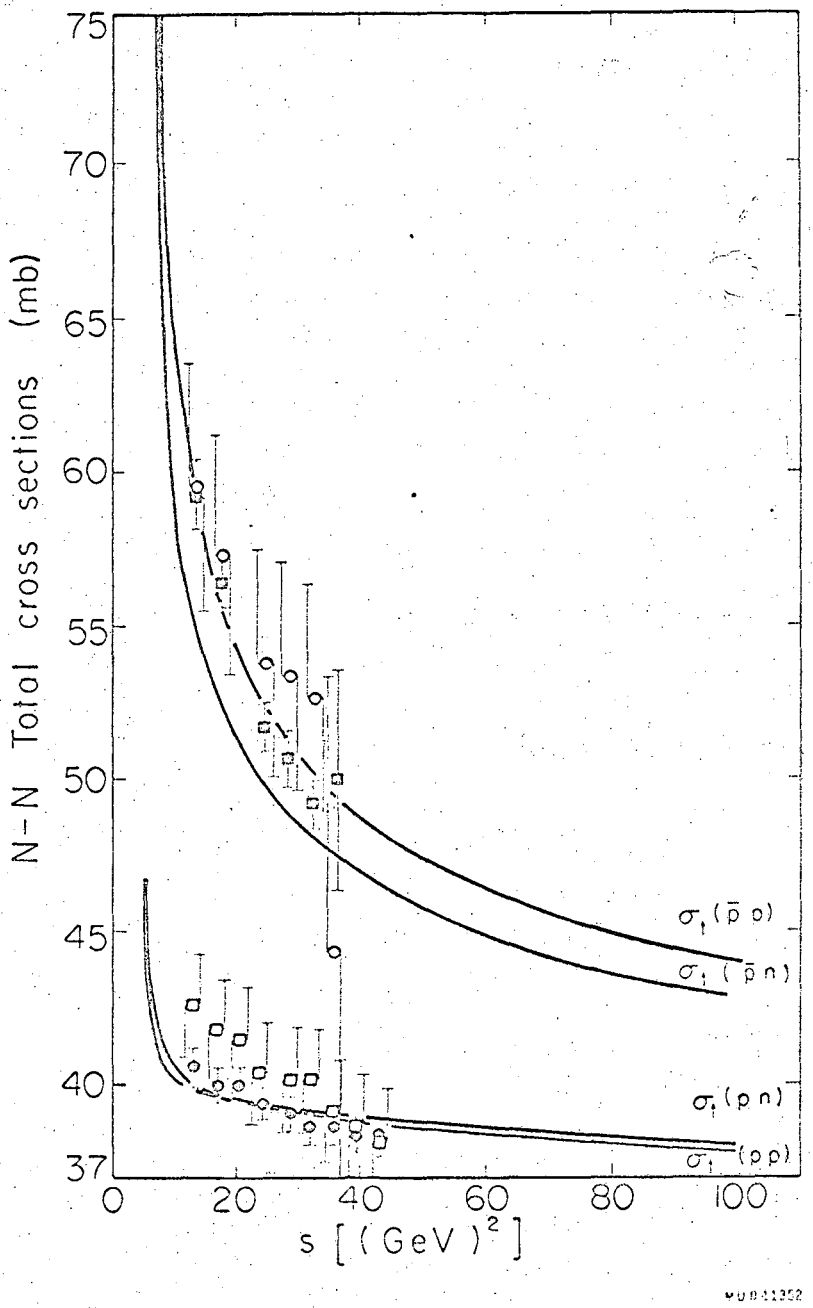
N-N Total cross sections (mb)
75
70
65
60
55
50
45
40
37
0
20
40
60
80
100
s [(GeV)²]
σt(p̄p)
σt(p̄n)
σt(pn)
σt(pp)

Fig. 2.

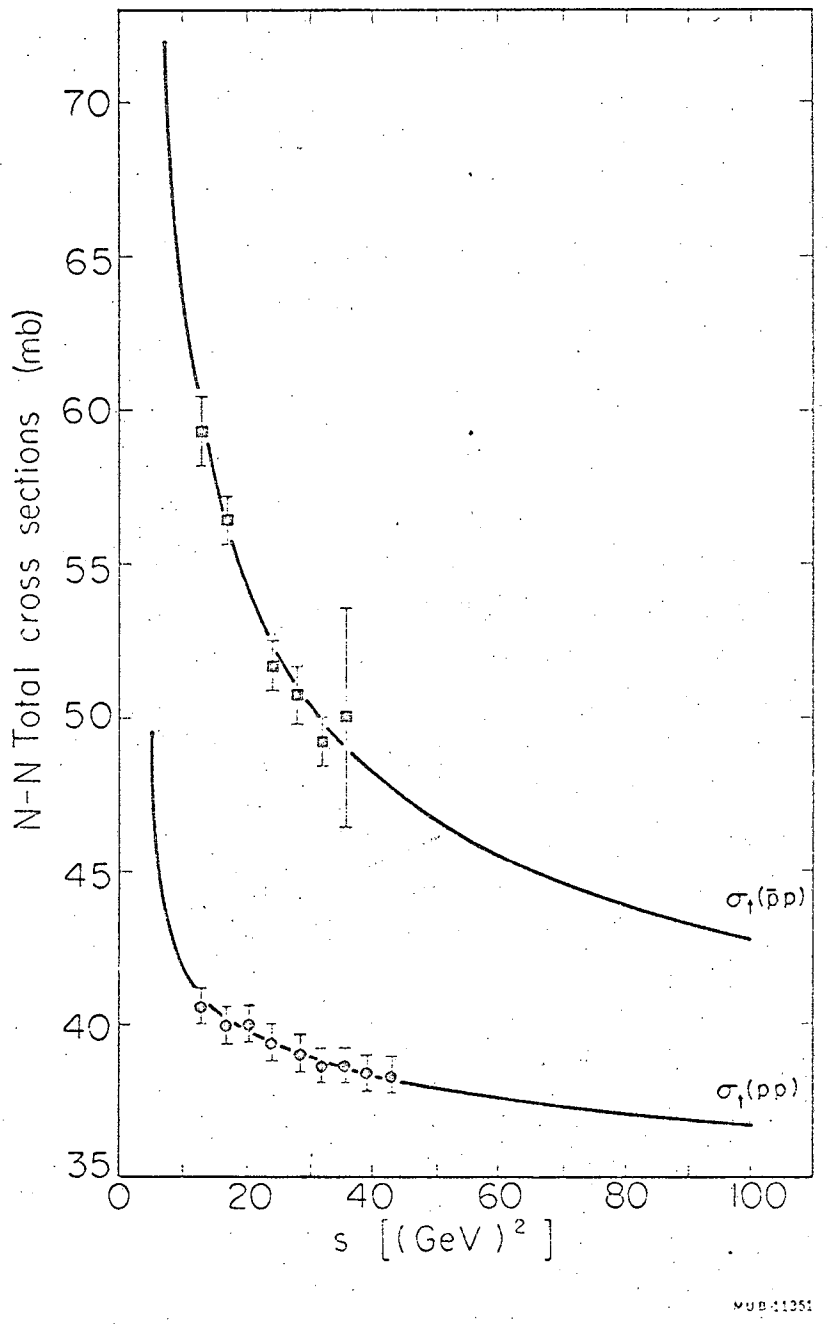
N-N Total cross sections (mb)
70
65
60
55
50
45
40
35
0
20
40
60
80
100
s [(GeV)²]
σ₁(p̄p)
σ₁(pp)
MUB-11351

Fig. 3.

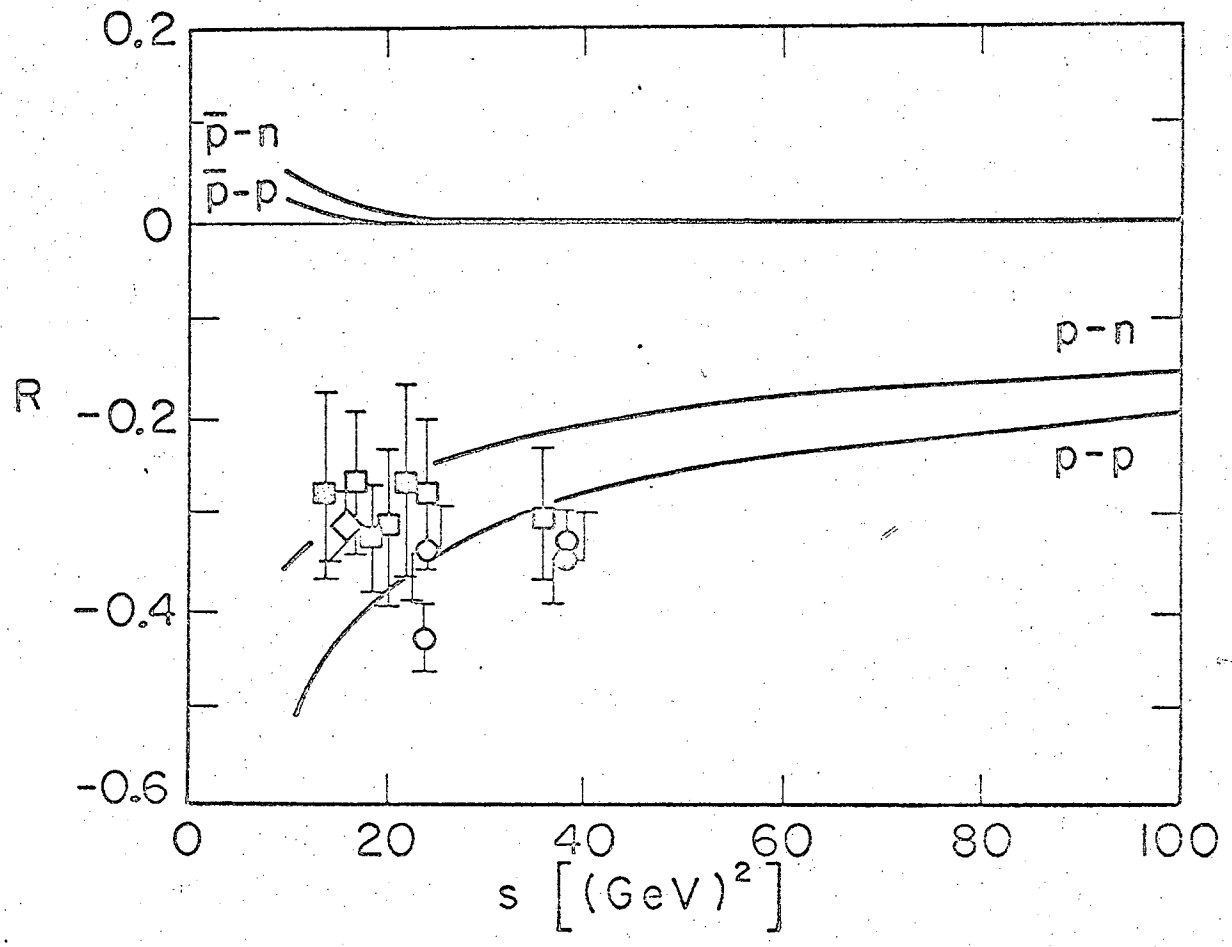

Fig. 4.

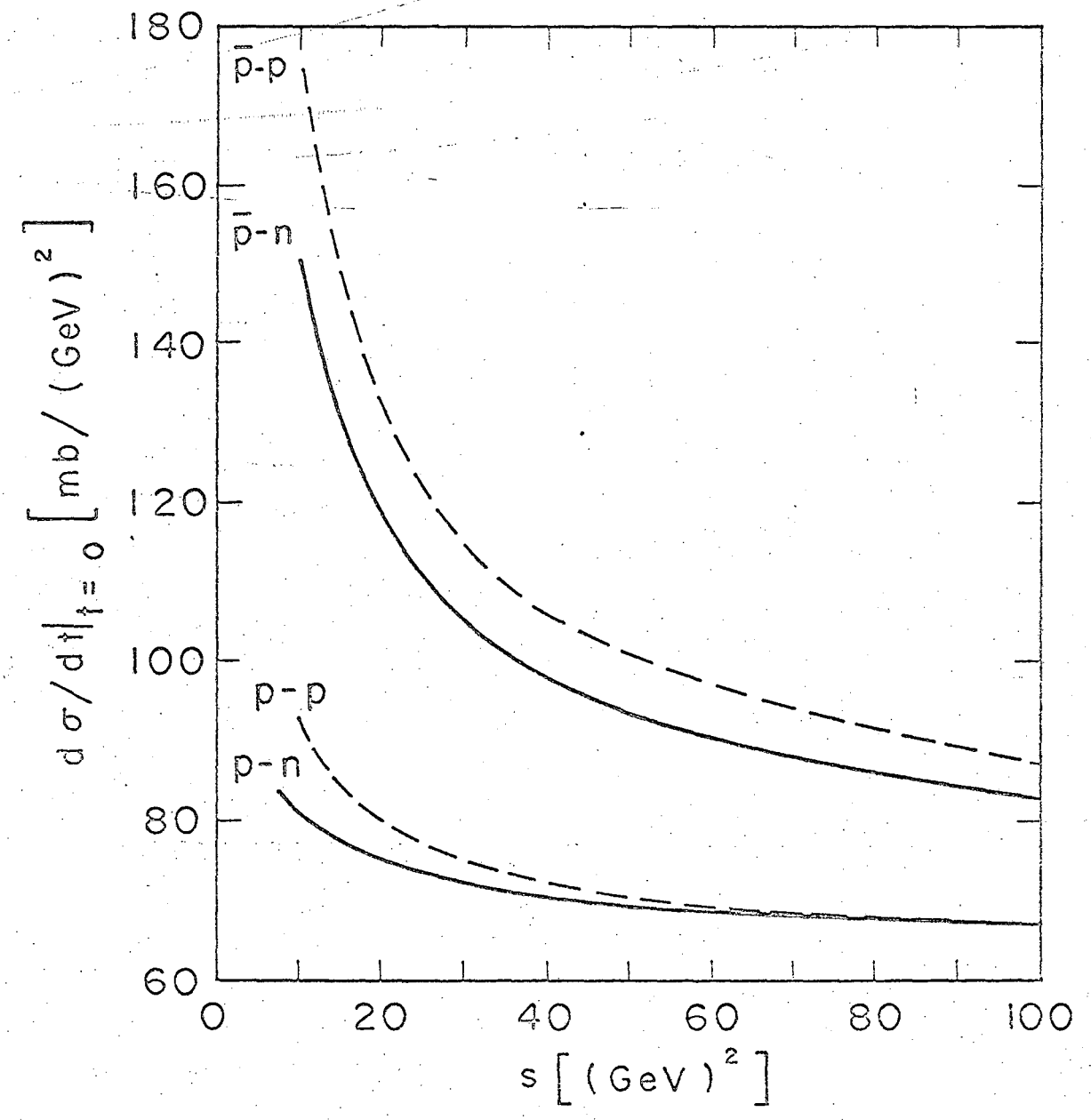
180
160
140
120
100
80
60
0
20
40
60
80
100
p̄-p
p̄-n
p-p
p-n
dσ/dt|t=0 [mb/(GeV)²]
s [(GeV)²]
MUB-11356

Fig. 5.

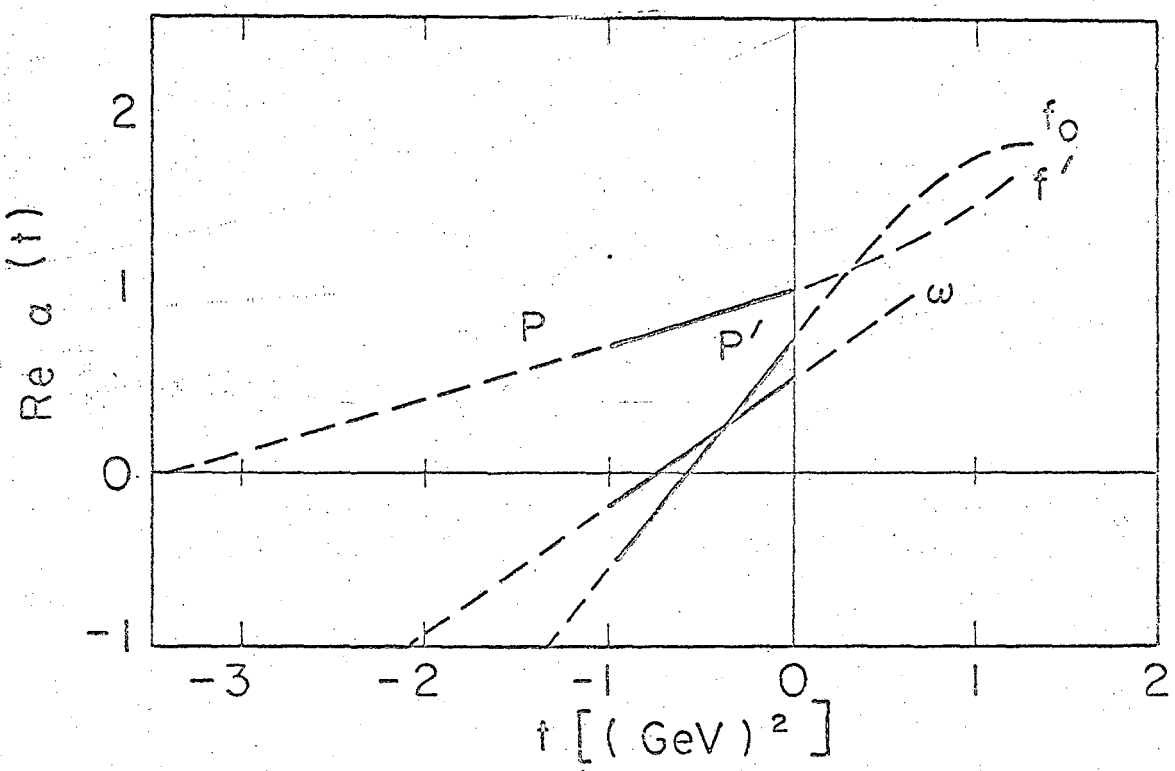

MUB-11355

Fig. 6.

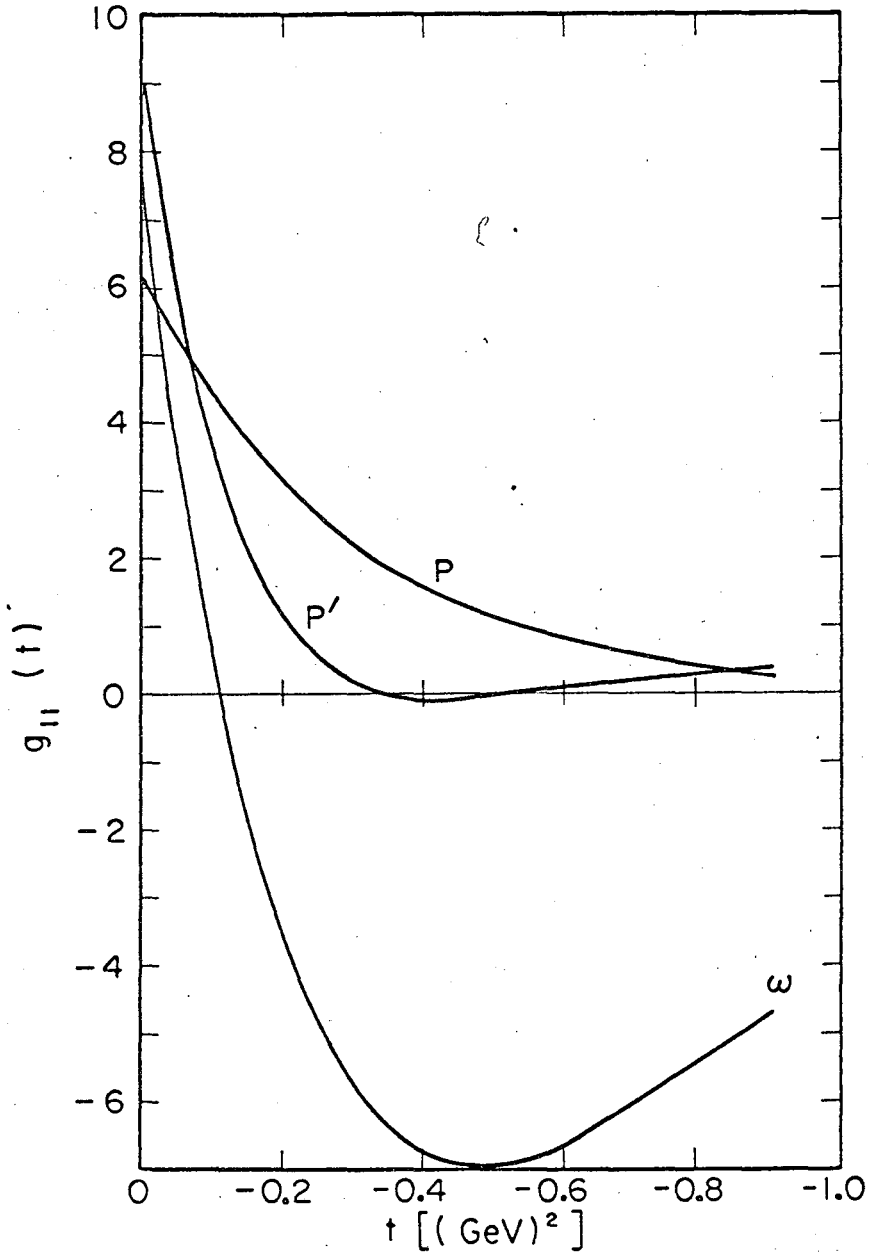

Fig. 7.

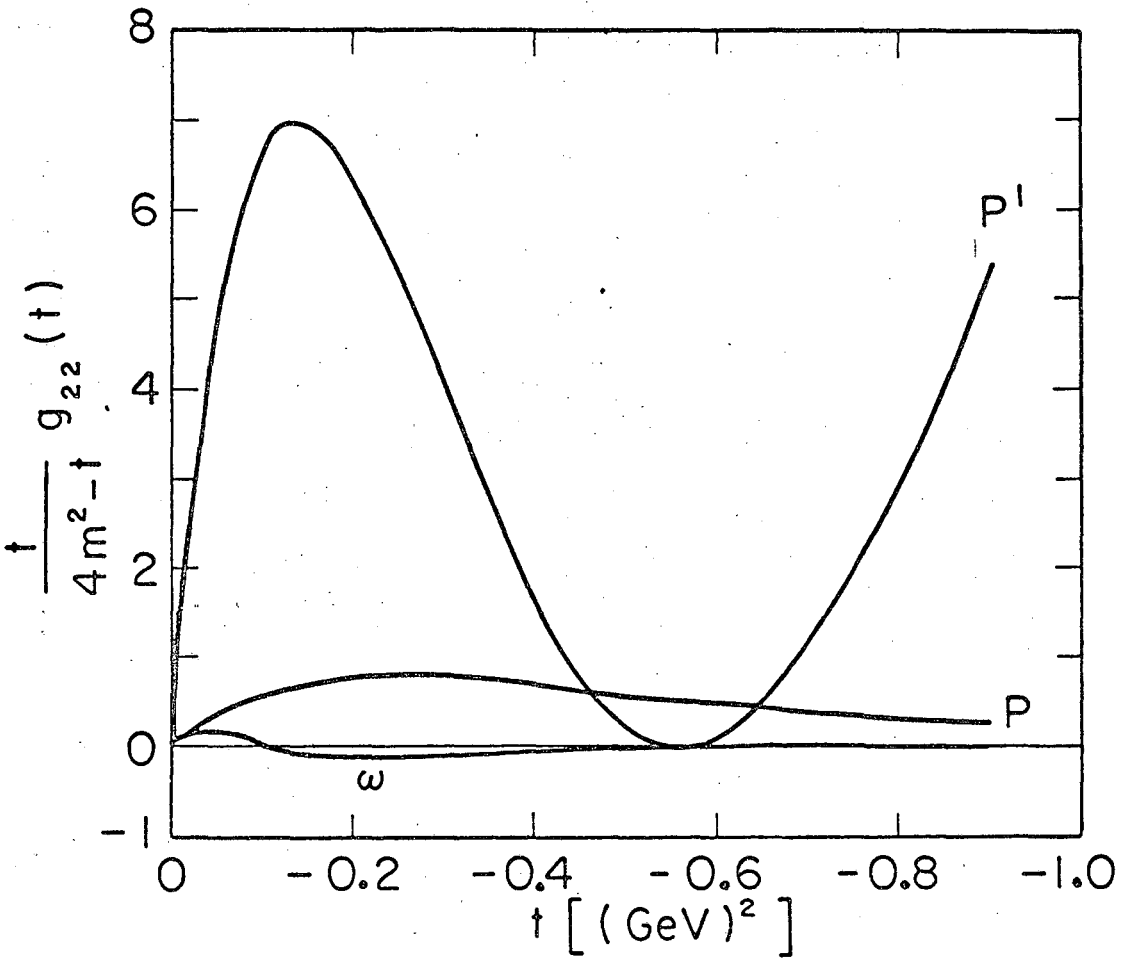

MUB-11358

Fig. 8.

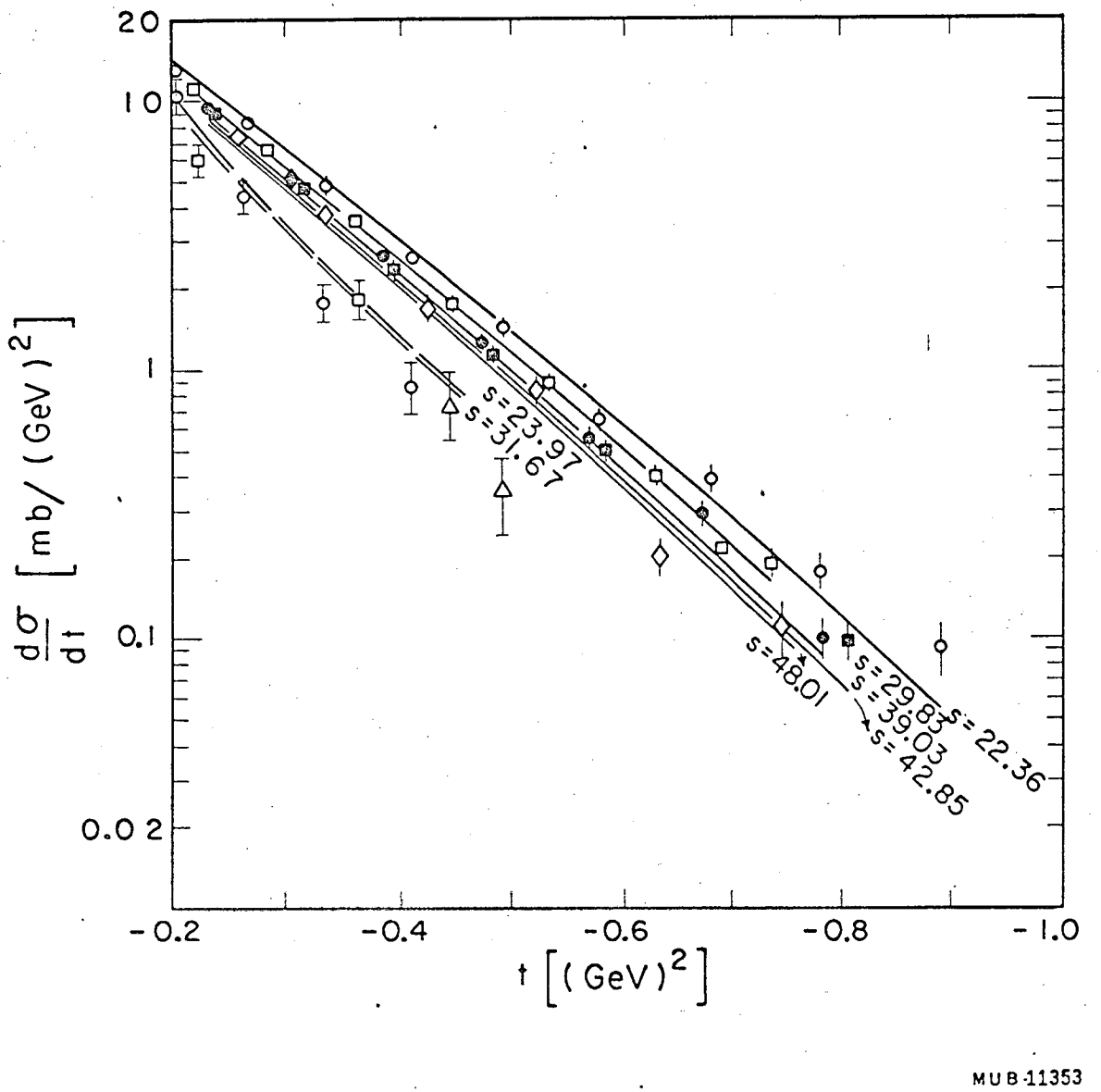
20
10
1
0.1
0.02
$\frac{d\sigma}{dt}$ [mb/(GeV)^2]
-0.2
-0.4
-0.6
-0.8
-1.0
t [(GeV)^2]
s=22.36
s=29.83
s=39.03
s=42.85
s=48.01
s=23.97
s=31.67
MUB-11353

Fig. 9.

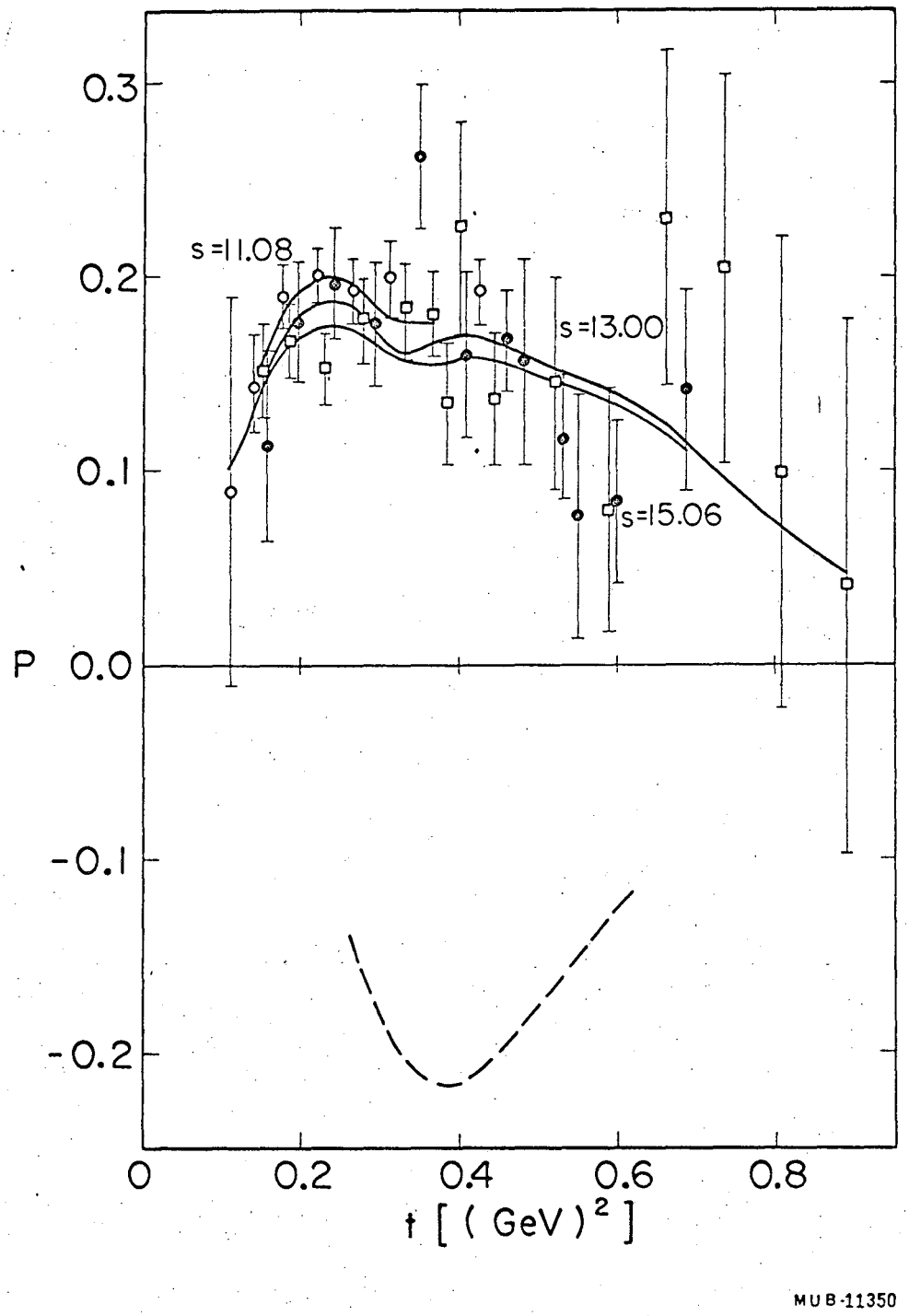
0.3
0.2
0.1
P 0.0
-0.1
-0.2
0
0.2
0.4
0.6
0.8
t [(GeV)^2]
s=11.08
s=13.00
s=15.06
MUB-11350

Fig. 10.

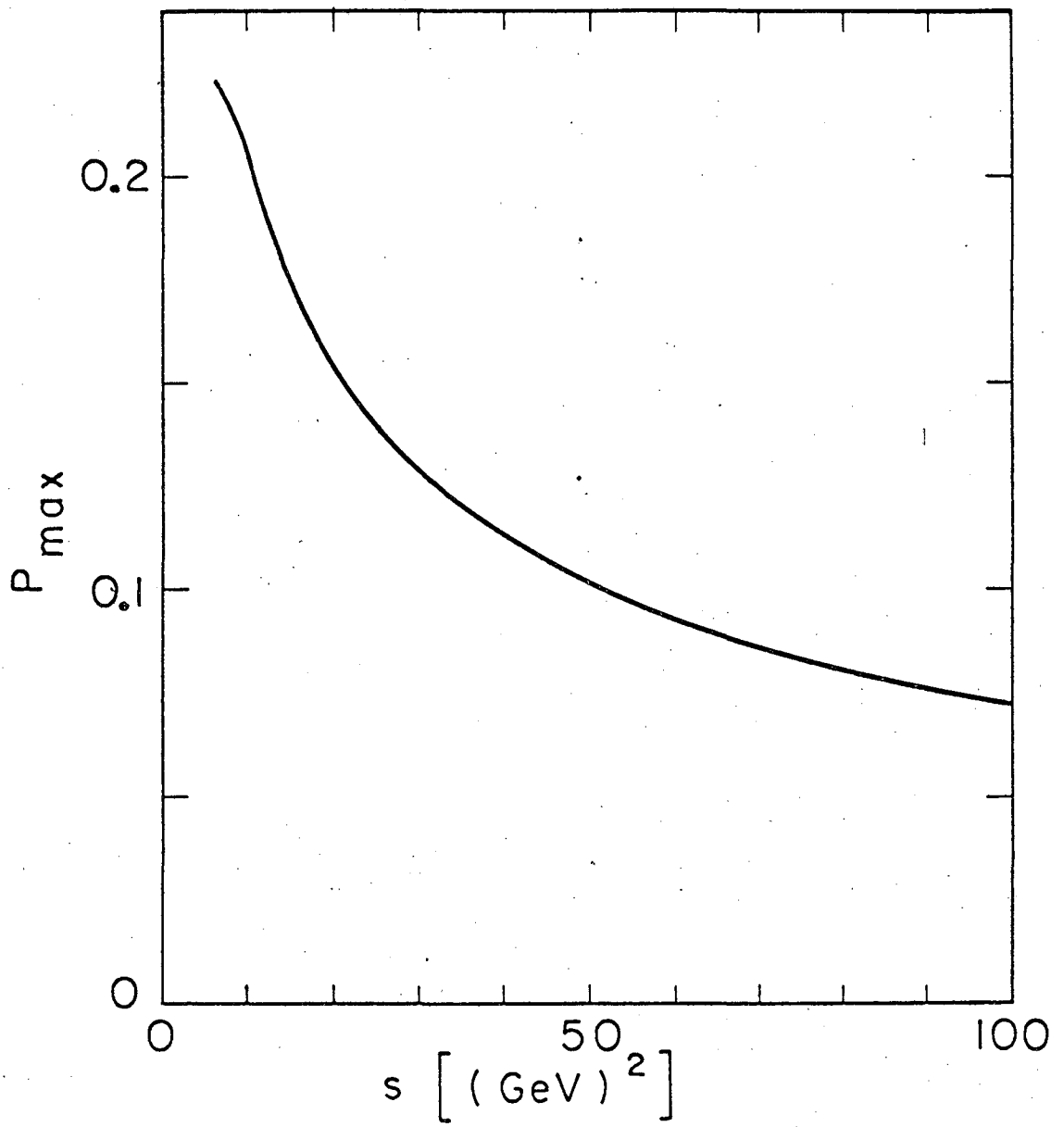

Fig. 11.

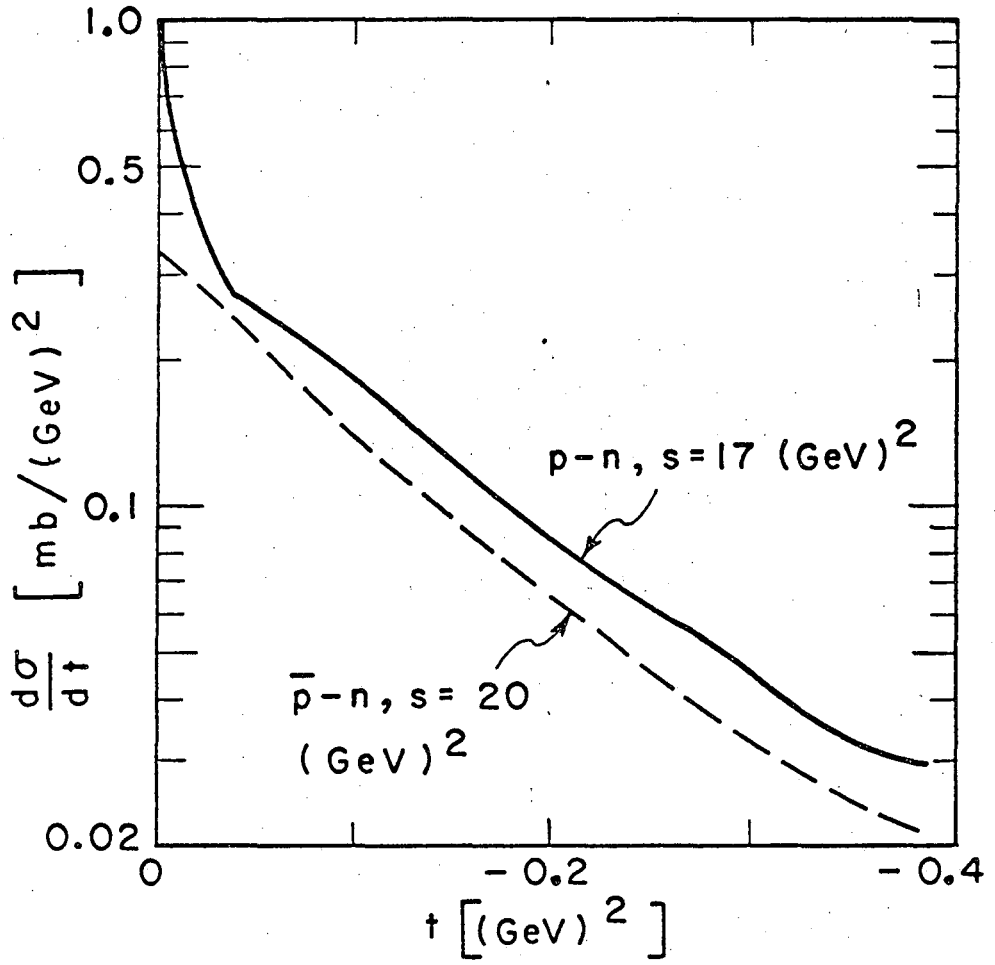

MUB-11359

Fig. 12.

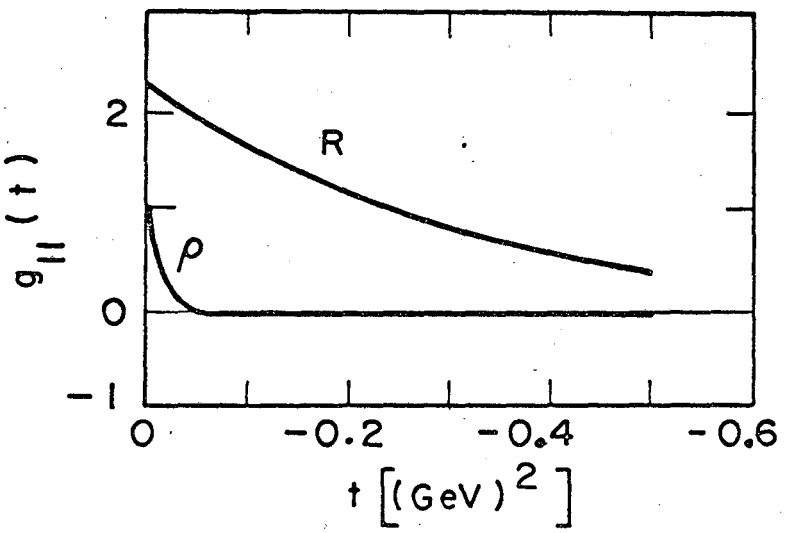

MUB-11360

Fig. 13.

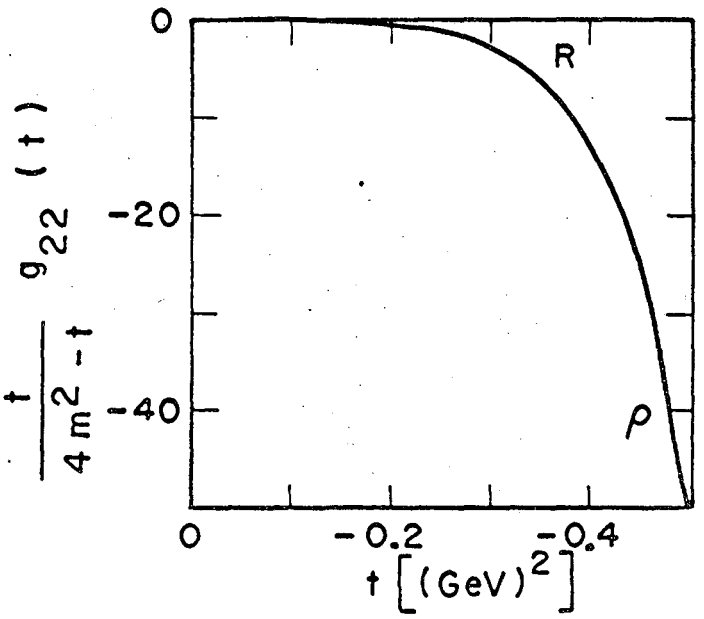

MUB-11363

Fig. 14.